RESEARCH ACTIVITIES VI
Department of Vacuum UV Photoscience

VI-A Electronic Structure and Decay Mechanism of Inner-Shell Excited Molecules

This project is being carried out in collaboration with Fritz-Haber Institute, McMaster University, University of Alberta, and Photon Factory. We are experimentally interested in ionic fragmentation and electron emission via inner-shell excitation of molecules and in their linear polarization dependence. Recently we are also developing a theoretical approach based on quantum chemistry for inner-shell spectroscopy and dynamics.

VI-A-1 Partial Electron Yield Spectrum of N_2: Doubly Excited States at the K-Shell Threshold

NEEB, Matthias[1]; BRADSHAW, Alexander M.[1]; KOSUGI, Nobuhiro
([1]Fritz-Haber Inst.)

[*Chem. Phys. Lett.* in press]

Doubly excited states have been revealed both below and immediately above the core ionization threshold in N_2 by measuring a partial electron yield spectrum at the kinetic energy corresponding to the Auger decay of the double excitations. In this partial yield spectrum the core-to-Rydberg transitions and the σ^* shape resonance are absent from this absorption spectrum. The calculated potential energy curves suggest a strongly dissociative nature of the molecular-type double excitations. This agrees well with the observed width of the absorption feature in the partial yield spectrum.

VI-A-2 Inner-Shell Excitation of PF_3, PCl_3, PCl_2CF_3, OPF_3 and SPF_3

NEVILLE, John J.[1]; JÜRGENSEN, Astrid[2]; CAVELL, Ronald G.[2]; KOSUGI, Nobuhiro; HITCHCOCK, Adam P.[1]
([1]McMaster Univ.; [2]Univ. Alberta)

[*Chem. Phys.* **238**, 201 (1998)]

Total ion yield spectra of PF_3, PCl_3, PCl_2CF_3, OPF_3 and SPF_3 were recorded in the region P 2p, P 2s, S 2p, S 2s and halogen (Cl 2p, F 1s) excitation using synchrotron radiation. The theoretical calculations indicate that several of the discrete states are best described as LS-coupled states because the core-valence electron exchange is very large and thus the singlet-triplet splitting is larger than the spin-orbit splitting. Aspects of partial ion yield measurements support this interpretation by revealing isolated single states without a corresponding partner at the spin-orbit splitting. The partial ion yields help clarify spectral interpretation by removing interference from overlap with adjacent states having the normal (j,j)-coupled ion core character.

VI-A-3 The Sulphur 2p Photoabsorption Spectrum of NSF_3

JÜRGENSEN, Astrid[1]; KOSUGI, Nobuhiro; CAVELL, Ronald G.[1]
([1]Univ. Alberta)

[*Chem. Phys.* in press]

The Sulfur 2p photoabsorption spectrum of gaseous NSF_3 has been measured at high resolution using synchrotron radiation. Similar to isoelectronic OPF_3 and other pyramidal phosphorus compounds there exist two states, best described as LS-coupled because of a very large core-valence electron exchange. The post-edge features, corresponding to outer well p and d shape resonances, were assigned.

VI-A-4 Jahn-Teller Effect and Rydberg-Valence Mixing in the C1s $\rightarrow$ 3pt_2 and 3dt_2 Rydberg Excited States of CH_4

ADACHI, Jun-ichi; TAKATA, Yasutaka; SHIGEMASA, Eiji; KOSUGI, Nobuhiro; YAGISHITA, Akira[1]
([1]KEK-PF)

Figure 1 shows angle-resolved photoion-yield spectra for the C1s excited states of CH_4 using linearly polarized synchrotron radiation. The angular distributions of fragment ions emitted from the C1s $\rightarrow$ 3pt_2 and 3dt_2 Rydberg excited states of CH_4 are anisotropic; the anisotropy parameter β_{3V} deviates from zero. This means that the bond angle on the fragmentation is distorted. The anisotropic photoabsorption is attributed to the Jahn-Teller effect in the excited states with $^1T_2$ symmetry. The bond angle distortion on the fragmentation is related to the Jahn-Teller distortion along the bending modes (ν_2 and ν_4). The Jahn-Teller effect in the Rydberg excited states is expected to be so weak that the T_d geometry is hardly changed. We have to take into accout the Rydberg-valence mixing in order to explain the present result, that is, the 2t_2* valence orbital may be mixed with the 3pt_2 and 3dt_2 Rydberg orbitals in the distorted geometry.

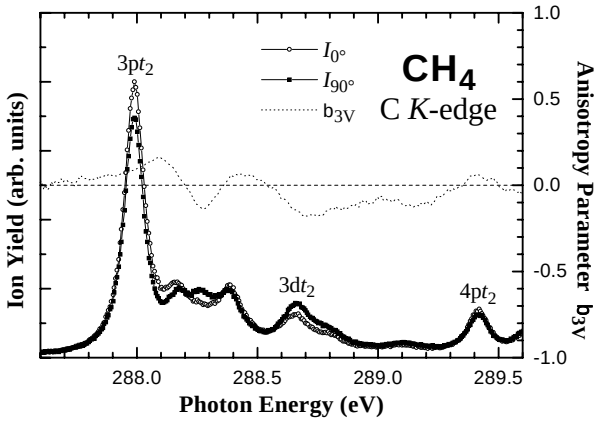

Figure 1. Angle-resolved ion-yield spectra for the C1s → $3pt_2$ and $3dt_2$ Rydberg excited states of CH_4.

VI-A-5 Renner-Teller Spliting in the 1s → $1\pi_g$* Excited States of C_2H_2

ADACHI, Jun-ichi; TAKATA, Yasutaka; SHIGEMASA, Eiji; KOSUGI, Nobuhiro; YAGISHITA, Akira[1]
([1]KEK-PF)

Figure 1 shows high-resolution angle-resolved photoion-yield spectra for the C1s → $1\pi_g$* excited states of C_2H_2. The π* peak shows fine structures on the lower energy side with a spacing of about 0.11 eV. The fine structures of the lower eneryg side are dominated by the bending modes (cis- and trans-bending modes), which are induced by the Renner-Teller effect. The fragment ions at the π* peak are observed not only in the 90° direction but also in the 0° direction ($I_{0°}$) respective to the electric vector of the incident light ($I_{90°}$); the anisotropy parameter β_{3V} deviates from –1. In addition, the $I_{0°}$ yield is slightly enhanced on the lower energy side of the peak. The result agrees with the Renner-Teller splitting, that is, the lower π* excited state has a stable bent structure. The π* peak has a clear shoulder structure on the higher energy side with its spacing of about 0.46 eV. This shoulder is mainly attributed to the C-H stretching mode.

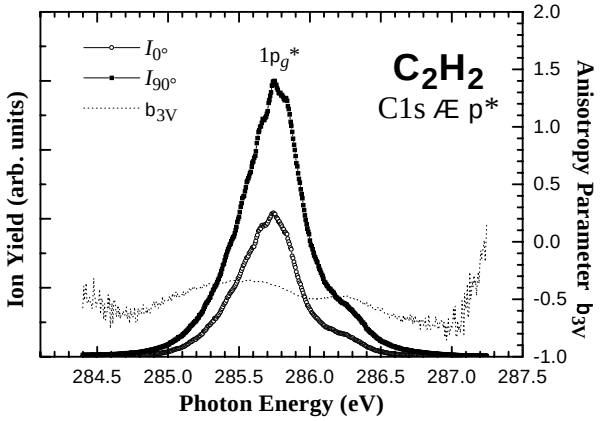

Figure 1. Angle-resolved ion-yield spectra for the C1s → π* states of C_2H_2.

VI-A-6 Enhancement of the O1s → nsσg Rydberg Series of CO_2 through the $5\sigma_g$-Valence Mixing

ADACHI, Jun-ichi; TAKATA, Yasutaka; SHIGEMASA, Eiji; KOSUGI, Nobuhiro; YAGISHITA, Akira[1]
([1]KEK-PF)

We have measured high-resolution angle-resolved ion-yield spectra for the O1s excited states of CO_2 using linearly polarized synchrotron radiation. The spectra show the $2\pi_u$* peak at 535.4 eV, the Rydberg series between 536 and 540.8 eV, the broad peak just above the O1s ionization threshold, and the shape resonance ($4\sigma_u$*) at 559 eV. It is found that the O1s → $3s\sigma_g$ Rydberg peak overlaps with the higher energy-side component of the π_u* peak. The present spectra show that the $ns\sigma_g$ Rydberg series is the stronger than the other Rydberg series. In addition, the intensity of the $4s\sigma_g$ Rydberg peak is stronger than that of the $3s\sigma_g$ Rydberg peak. These results are explained by the $ns\sigma_g$ Rydberg-$5\sigma_g$* valence mixing as in the case for the terminal N and O1s excited states of N_2O.[1)] On the other hand, the $5\sigma_g$* valence excited state may raise its energy just above the O1s ionization threshold through the mixing.

Reference
1) J. Adachi *et al.*, *J. Chem. Phys.* **102**, 7369 (1995).

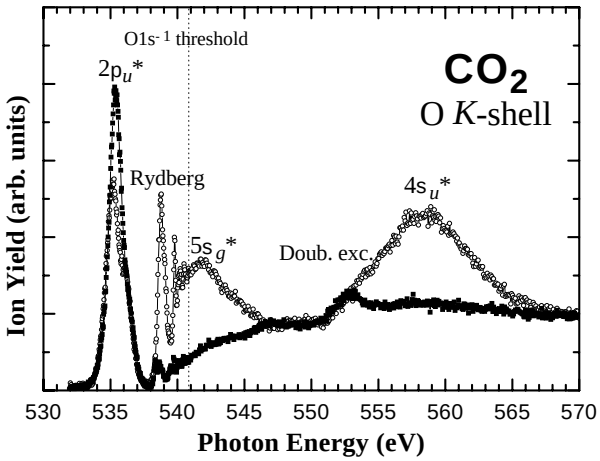

Figure 1. Angle-resolved ion-yield spectra for the O1s excited states of CO_2.

VI-A-7 Vibronic Coupling and Valence Mixing in the 1s → Rydberg Excited States of C_2H_2 in Comparison with N_2 and CO

ADACHI, Jun-ichi; SHIGEMASA, Eiji; KOSUGI, Nobuhiro; YAGISHITA, Akira[1]
([1]KEK-PF)

[*Chem. Phys. Lett.* in press]

The angle-resolved ion-yield spectra are reported for the C1s → Rydberg excitations of linear acetylene, C_2H_2, in comparison with N_2 and CO. The $3\sigma_u$* valence state is observed in the $3s\sigma_g$ Rydberg region with no mixing. The $3p\sigma_u$ state is found in the same region as the C1sσ_g → $3p\pi_u$ state, which shows only totally symmetric vibrations. This is the first to observe that the Rydberg state in C_2H_2 keeps gerade and ungerade symmetries without vibronic coupling through

antisymmetric stretching vibrations related to core hole localization. On the other hand, the lowest $1\pi_g$* valence state induces vibronic coupling through bending vibrations in the $3\sigma_u$* and $3s\sigma_g$ states.

VI-B Soft X-Ray Photoelectron-Photoabsorption Spectroscopy and Electronic Structure of Transition Metal Compounds

We are investigating electronic structure of molecular Ni complexes with planar structure by means of inner-shell photoabsorption and photoelectron spectra at the soft X-ray double crystal monochromator beamline BL1A of the UVSOR facility. We have found that a one-electron picture is appropriate to interpret the Ni 2p photoabsorption and resonant photoelectron spectra of the molecular Ni complexes, and that the metal-to-ligand charge transfer (MLCT) is essential to describe the photoexcited states. This year, we extend our study to resonant X-ray emission spectra, and also to another Ni compounds with Ni-Ni bonding.

VI-B-1 Ni 2p-3d Photoabsorption and Strong Charge Transfer Satellites in Divalent Ni Complexes with Molecular Ligands. Evaluation of π-Back Donation Based on the DFT Approach

PETTERSSON, Lars G. M.; HATSUI, Takaki[1]; KOSUGI, Nobuhiro
([1]GUAS)

[*Chem. Phys. Lett.* in press]

Density functional theory within a transition potential approach (DFT-TP) is applied to interpret remarkably strong π-type MLCT (metal-to-ligand charge transfer) satellites in the Ni 2p photoabsorption of planar low-spin Ni^{II} complexes, $K_2Ni(CN)_4 \cdot H_2O$ and bis(dimethylglyoximato)nickel. The MLCT intensities calculated with DFT-TP are in good agreement with experiment, whereas the HF-STEX (Hartree-Fock based static exchange approximation) approach underestimates the intensities. The DFT-TP approach gives more reasonable π-back donation due to a better description of the strong covalency hybridization of the ligand π* orbitals with the occupied 3d orbitals. The DFT analysis indicates that we can evaluate π-back donation qualitatively by experimentally examining the MLCT satellites.

VI-B-2 Ni-Ni Chemical Bond in $[Ni_2(napy)_4Br_2]$-$[B(C_6H_5)_4]$ Studied by Linearly Polarized Ni 2p Photoabsorption

HATSUI, Takaki[1]; TAKATA, Yasutaka; KOSUGI, Nobuhiro
([1]GUAS)

The Ni-Ni bonding is not well characterized in contrast to the metal-metal bonds of early transition metals. In order to elucidate the character of Ni-Ni bonding, linearly polarized Ni 2p photoabsorption spectra of $[Ni_2(napy)_4Br_2][B(C_6H_5)_4]$ (napy: 1,8-naphthyridine) were measured (Figure. 1). For $[Ni_2(napy)_4Br_2]^{1+}$ cation with Ni atoms of the formal oxidation number +1.5, there are 3 holes in σ–, δ–, and π–symmetry orbitals produced mainly by Ni 3d orbitals. The lowest band A is strong in the E ⊥ z direction, and very weak in the E // z direction, where E and z denote the electric vector of the incident photon and the molecular axis parallel to the Ni-Ni bond, respectively. This indicates that some holes are located in δ orbitals. On the contrary, band B is strong in the E // z direction and weak in the E ⊥ z direction, indicating that the other holes are located in the σ* orbital. The intensity ratio of band A to B is estimated to be about 2 from the spectrum of the powder sample. Therefore, one hole is located in the σ* orbital and two holes in δ-symmetry orbitals, though we cannot distinguish between $\delta^3\delta^{*3}$ and $\delta^4\delta^*$ configurations.

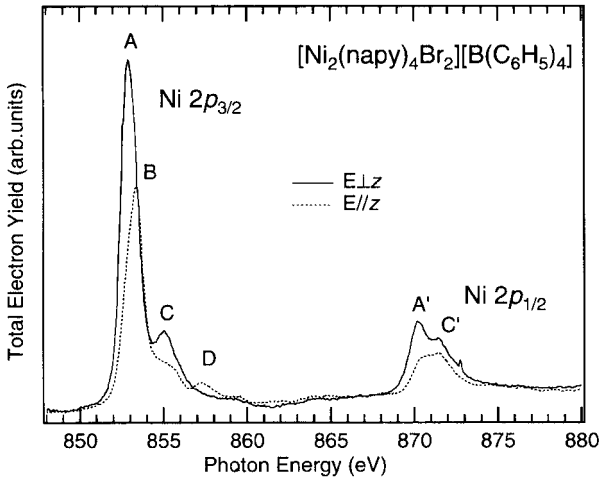

Figure 1. Linearly polarized Ni 2p photoabsorption spectra of a single crystalline $[Ni_2(napy)_4Br_2][B(C_6H_5)_4]$ for the E // z and E ⊥ z directions, where E and z denote the electric vector of the incident photons and the molecular axis z parallel to the Ni-Ni bond, respectively.

VI-B-3 Valence Band Excitation Observed in Resonant Soft X-Ray Emission Spectra of $K_2Ni(CN)_4 \cdot H_2O$ at the Ni 2p Edge

TAKATA, Yasutaka; HATSUI, Takaki[1]; KOSUGI, Nobuhiro; AGUI, Akane[2]; MAGNUSON, Martin[2]; SATHE, Conny[2]; RUBENSSON, Jan-Erik[2]; NORDGREN, Joseph[2]
([1]GUAS; [2]Uppsala Univ.)

In order to investigate the valence band structure of a planar nickel complex $K_2Ni(CN)_4 \cdot H_2O$, which shows

characteristic MLCT (metal-to-ligand charge transfer) bands in the Ni 2p photoabsorption spectra, resonant soft X-ray emission spectra at the Ni 2p edge have been measured. The experiments were performed at the undulator beamline BW3 in HASYLAB (Germany).

Soft x-ray emission spectra of $K_2Ni(CN)_4 \cdot H_2O$ at some Ni 2p resonant excitation are plotted in Figure 1 as a function of the energy difference between excitation and emission energies. At resonance A assigned to the intra-atomic Ni 2p → 3d* excitation, three structures are observed in addition to the elastic peak at 0 eV. These peaks correspond to the d → d* valence excitation with different symmetry. On the other hand, at t resonances B and C, the spectra drastically changed and give the single peak with narrow band width. We have assigned resonances B and C to the excitation to ligand π* orbitals with different symmetry; therefore, the emiision peaks correspond to the d → π* or π → π* valence excitation.

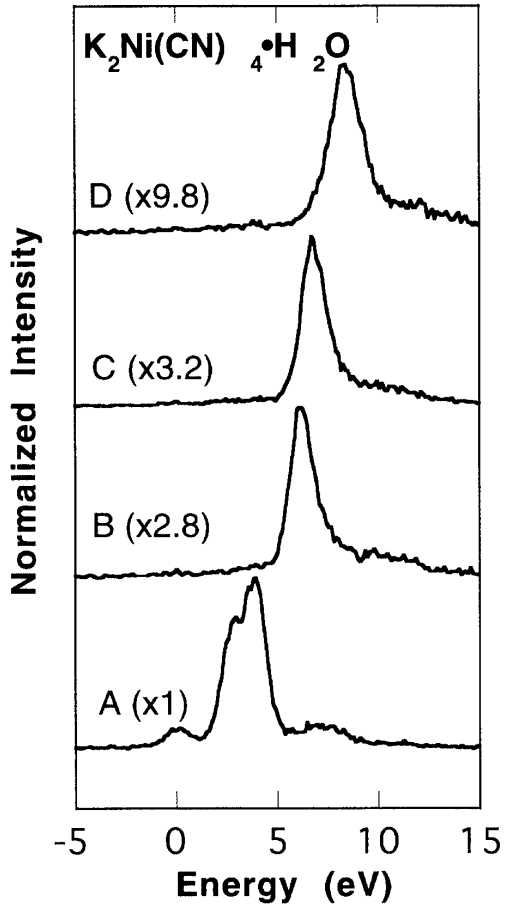

Figure 1. Soft x-ray emission spectra of $K_2Ni(CN)_4 \cdot H_2O$ at some Ni 2p resonant excitation The energy (lateral axis) is obtained by subtracting the emission energy from the excitation energy.

VI-B-4 Resonant X-Ray Emission Spectra of $K_2Ni(CN)_4 \cdot H_2O$ at the Ni 1s Edge

TAKATA, Yasutaka; HATSUI, Takaki[1]; SHOJI, Hironobu[2]; IWAZUMI, Toshiaki[3]; KOSUGI, Nobuhiro
([1]GUAS; [2]Univ. Tokyo; [3]KEK-PF)

Recently, we have reported that the electronic structure of nickel planar complexes can be described within a one-electron picture from the Ni 2p photoabsorption and resonant photoelectron spectra. This is different from the interpretation for the strongly correlated system such as NiO. In order to confirm our interpretation experimentally, resonant X-ray emission spectra of $K_2Ni(CN)_4 \cdot H_2O$ at the Ni 1s edge were measured at the beamline BL-8B in Photon Factory.

Figure 1 shows resonant X-ray emission spectra at the Ni 1s excitation. The spectrum A was measured at a quadrupole transition to Ni $3d_{x2-y2}$, and B, C are at dipole transitions to Ni 4pπ*. The elastic peak is shifted to the higher energy side with increase of the excitation energy. Nearby the peak, no extra feature with energy loss was observed. This is quite different from the results for NiO. In NiO, two peaks with the energy loss of 4.9 and 7.8 eV were observed and assigned to the deexcitation to an LMCT (ligand-to-metal charge transfer) state $3d^9\underline{L}$ ($\underline{L}$: ligand hole). The absence of the energy loss feature clearly indicates that LMCT is not important and the one-electron picture is appropriate for the nickel planar complexes. For the Ni K_β line, the energy shift is observed, depending on the photoexcited states. Narrowing of the peak width due to the Raman effect was observed.

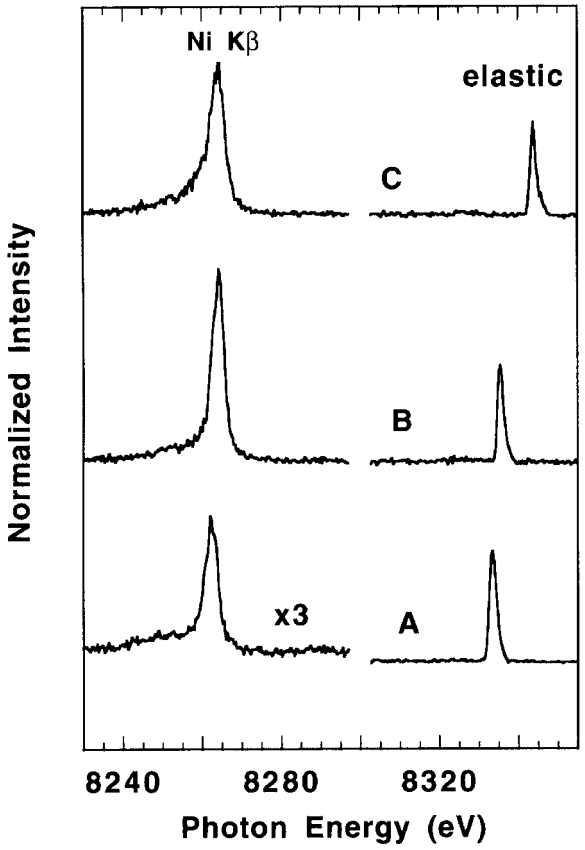

Figure 1. X-ray emission spectra of $K_2Ni(CN)_4 \cdot H_2O$ at Ni 1s edge.

VI-C Generation of Ultrashort Optical Pulse for Time-Resolved Spectroscopy

It is important to improve time-resolution of time-resolved spectroscopy because higher time-resolution gives us a chance to observe new "fast" phenomena that can not be recognized with lower time-resolution. Nowadays, we can generate sub-10 fs pulses using modern laser technology. Although it is not easy task to handle such short optical pulses and to employ them for the study in molecular science, time-resolved spectroscopy utilizing such pulses are very important and desirable. We constructed two optical setups to generate ultrashort optical pulses whose duration is in the range from ten to a few tens of femtoseconds.

VI-C-1 Development of UV-Excited Transient Absorption Spectrometer Based on 10-fs Pulses

TAKEUCHI, Satoshi; TAHARA, Tahei

Ultrashort optical pulses have been widely used in time-resolved spectroscopic studies of the excited state properties and the reaction dynamics of molecules. The time-resolution in most of these studies, however, has been so far limited to the range of 200–500 fs. Particularly in experiments using ultraviolet pulses, the time-resolution tends to become worse due to broadening of the pulse duration in the frequency conversion process to the ultraviolet. In this project trying to achieve better time-resolution in molecular spectroscopy, we have constructed a high-power optical parametric amplifier (OPA) producing 10-fs pulses in the visible region, and utilized it for the transient absorption measurements (Figure 1). In the OPA, a femtosecond white-continuum seed pulse is amplified twice in a BBO nonlinear crystal, which is pumped by the second harmonic (400 nm) of the amplified Ti:sapphire laser pulse. The output pulse is then sent to a double-pass prism compressor to correct its phase dispersion. The autocorrelation of the compressed pulse (Figure 2A) indicates that the pulse duration is as short as 9.6 fs. The OPA is tunable in the wavelength region of 500–750 nm, and the typical pulse energy is 10–15 μJ at a 1 kHz repetition rate. Next, in the transient absorption spectrometer, most of the 10-fs pulse energy from the OPA is focused into a thin BBO crystal to generate the second harmonic tunable in the near-ultraviolet (250–375 nm). After the phase-dispersion compensation with a prism pair, the second harmonic is used as a pump pulse for photoexcitation of the sample. The minor rest of the 10-fs pulse is used as a probe and a reference pulse. The time-resolution of this spectrometer is evaluated as 35 fs from a cross-correlation trace between the pump and probe pulses (Figure 2B). This value is an order of magnitude better than that of a conventional transient absorption spectrometer using femtosecond white-continuum pulses. Observation of the excited state dynamics in a very early time region is now in progress by using this spectrometer.

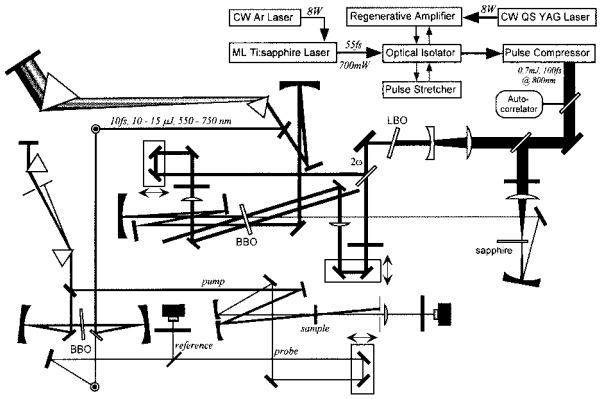

Figure 1. Experimental setup for uv-excited transient absorption measurements using 10-fs pulses.

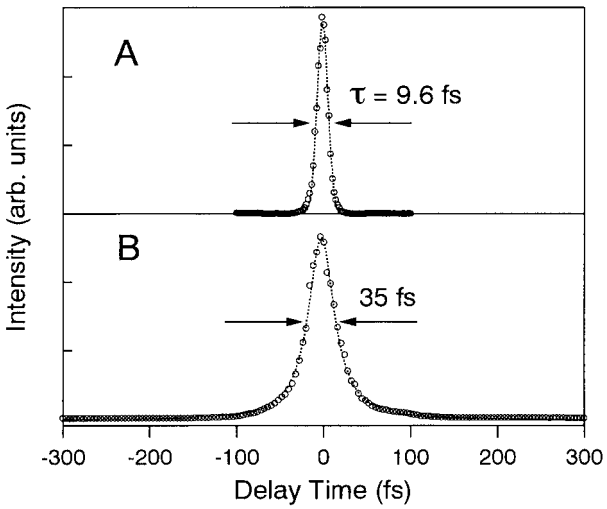

Figure 2. Autocorrelation of the OPA output pulse (A), and cross-correlation trace between the pump and probe pulses used in the transient absorption spectrometer (B).

VI-C-2 Generation of Ultra-Short Pulses Using a Krypton Gas-Filled Hollow Fiber

FUJIYOSHI, Satoru; TAKEUCHI, Satoshi; TAHARA, Tahei

We have constructed an apparatus to generate ultra-short pulses using a krypton gas-filled hollow fiber.[1)] This apparatus consists of two parts. In the first part, the femtosecond pulse from a Ti:sapphire regenerative amplifier (100 fs, 800 nm, 210 μJ, 1 kHz) is coupled into a hollow fiber that is filled with krypton gas. The input pulse spectrum becomes broader due to the self phase modulation in the gas while the pulse passes

through the fiber. The spectrum of the input pulse and that of the output pulse from the hollow fiber are shown in Figure 1a. Spectral width of the input pulse is 12 nm (FWHM) and that of the output pulse covers a wide range from 770 to 870 nm. In the second part, the broadened output pulse is sent to a prism compressor to correct its group velocity dispersion. Autocorrelation of the final compressed pulse is shown in Figure 1b. The pulse duration is as short as 30 fs as well as pulse energy of 5 μJ has been obtained.

Reference

1) M. Nisoli *et al.*, *Opt. Lett.* **22**, 522 (1997).

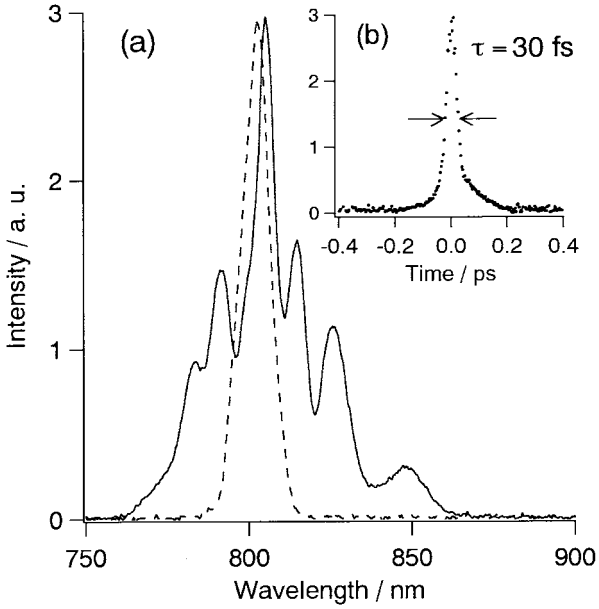

Figure 1. (a) Spectra of input pulse (dashed line) and output pulse (solid line) of hollow fiber. (b) Auto-correlation trace. The pulse duration (FWHM) is 30 fs.

VI-D Studies of Primary Photochemical/Physical Processes Using Femtosecond Fluorescence and Absorption Spectroscopy

Ultrafast spectroscopy is playing an essential role in elucidation of photochemical reactions. Thanks to the recent advance in laser technology, we are now able to observe the dynamics of chemical reactions taking place in the femtosecond time region. In this project, we are studying primary photochemical/physical processes in the condensed phase using time-resolved fluorescence and absorption spectroscopy with a few hundreds femtoseconds time-resolution. Time-resolved fluorescence and absorption spectroscopy are complimentary to each other. The advantage of fluorescence spectroscopy lies in the fact that fluorescence originates from the transition between the "well-known" ground state and the excited state in question. Thus time-resolved fluorescence spectroscopy can afford unique information not only about the dynamics but also other properties of the excited singlet states such as their energies and oscillator strengths. On the other hand, however, time-resolved absorption spectroscopy is considered to be more versatile because it can detect not only fluorescent excited singlet states but also other "dark" transients. In this year, we investigated the ultrafast proton transfer reaction and the relaxation process of the highly excited states of several fundamental molecules, with use of these time-resolved electronic spectroscopy.

VI-D-1 Vibronic Relaxation of Polyatomic Molecule in Non-polar Solvent: Femtosecond Anisotropy/Intensity Measurements of the S_n and S_1 Fluorescence of Tetracene

SARKAR, Nilmoni; TAKEUCHI, Satoshi; TAHARA, Tahei

[*J. Phys. Chem. A* **103**, 4808 (1999)]

The electronic and vibrational relaxation of tetracene have been studied in solution by femtosecond time-resolved fluorescence spectroscopy. Tetracene was initially photoexcited to the highly excited singlet (S_n) state, ^1B_b, and the dynamics of the fluorescence from the ^1B_b state and the ^1L_a state (S_1) were investigated by fluorescence up-conversion. The fluorescence from the ^1B_b state was observed in the ultraviolet region, and its lifetime was determined as ~120 fs. The anisotropy of the ^1B_b fluorescence was close to 0.4, which assured that the fluorescence is emitted from the excited state that was prepared by photoexcitation. The visible fluorescence from the ^1L_a state showed a finite rise that agreed well with the decay of the ^1B_b fluorescence (Figure 1A). Negative anisotropy was observed for the ^1L_a fluorescence, reflecting that the ^1L_a transition moment is parallel to the short axis of the molecule and hence perpendicular to the ^1B_b transition moment. The anisotropy of the ^1L_a fluorescence, however, showed a very characteristic temporal behavior in the femto-second time region: it exhibited a very rapid change and reached a certain value that is deviated from –0.2 (Figure 1B). The anisotropy data indicate that the ^1L_a fluorescence contains not only short-axis polarized component but also long-axis polarized component and that the ratio between the two components depends on both time and wavelength. The long-axis polarized component in the ^1L_a fluorescence was assigned to the

^1B_b-type fluorescence that appears as the result of the vibronic coupling between the ^1L_a state and the ^1B_b state. The observed initial rapid change of the anisotropy suggests that the highly excited vibrational states in the ^1L_a state which are strongly coupled with the ^1B_b state are first populated preferentially when the molecule is relaxed from the ^1B_b state to the ^1L_a state. The visible fluorescence anisotropy vanishes gradually due to the rotational diffusion in a few tens of picoseconds. In the picosecond region, we also observed additional dynamics in the fluorescence intensity whose time constant was about 12 ps. This dynamics was assigned to the vibrational relaxation (cooling) in the ^1L_a state. The observed relaxation processes that take place after photoexcitation of tetracene are sketched in Figure 2.

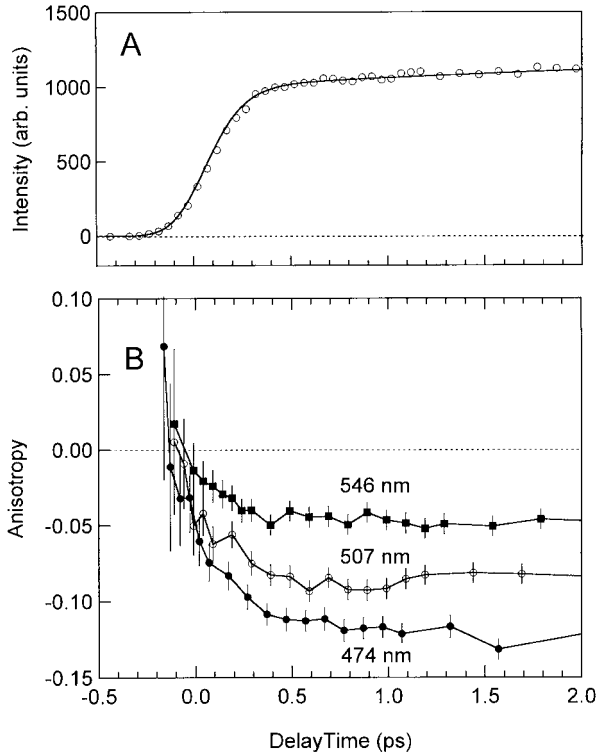

Figure 1. Early-time dynamics of the fluorescence intensity and anisotropy obtained from tetracene in hexadecane (273 nm excitation). (A) Time-resolved fluorescence signal at 507 nm measured with the magic angle condition. (B) Time-resolved fluorescence anisotropy measured at three different wavelengths (474, 507 and 546 nm).

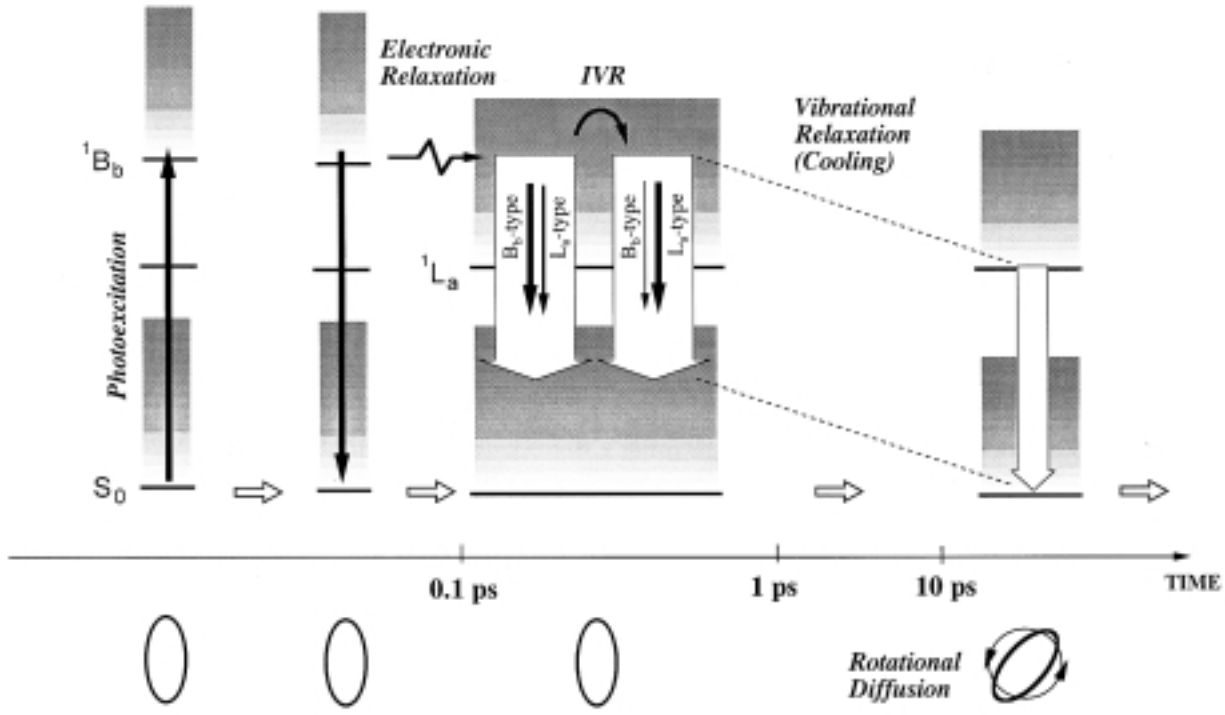

Figure 2. Schematic diagram depicting the relaxation processes of tetracene in solution following the direct photoexcitation to the highly excited singlet (S_n) state.

VI-D-2 Determination of the Excited-State Transition-Moment Directions of 7-Azaindole Dimer by Femtosecond Fluorescence Anisotropy Measurements

TAKEUCHI, Satoshi; TAHARA, Tahei

Time-resolved fluorescence anisotropy data can afford much information not only about the orientational diffusion of molecules in solution but also about the transition moment of the fluorescing state. In fact, the anisotropy change observed in the femtosecond time region does not arise from the orientational diffusion but is mainly caused by changes in the transition-moment direction, because the molecular motion is almost neglected in this short time region. Femtosecond fluorescence anisotropy measurement is, therefore, a powerful method which enables us to determine the transition-moment directions. In order to know the transition-moment directions of the three excited states (dimer L_b, dimer L_a, and tautomer L_a) which appear successively in the proton transfer reaction of 7-azaindole dimer, we measured fluorescence anisotropy of this dimer at three visible wavelengths with a 230-fs time-resolution (Figure 1). The anisotropy shows a rapid decay within one picosecond, and its feature depends on the observation wavelength. An additional slow component (12 ps) observed in every wavelength is due to the orientational diffusion of the dimer. We have simulated the time-dependence of the anisotropy on the basis of a model that includes the three excited states, and determined relative angles of the transition moments of each excited state by a fitting procedure (dotted curves). It was found that the wavelength dependence of the observed anisotropy can be explained by spectral difference of the fluorescences from the three excited states and that relative angle obtained from the data taken at the three wavelengths agreed very well with one another. We concluded that the relative transition-moment directions of the dimer L_a and tautomer L_a states with respect to the initially-populated dimer L_b state are 39° and 42°, respectively. It was reported by a rotational contour analysis of 7-azaindole in gas phase that the transition moment of the L_b state is 16° tilted from the inertial axis. Consequently, we can finally determine the absolute direction of the transition moments with respect to the inertial axis as 16°, 55°, and 58° for the dimer L_b, dimer L_a, and tautomer L_a states, respectively.

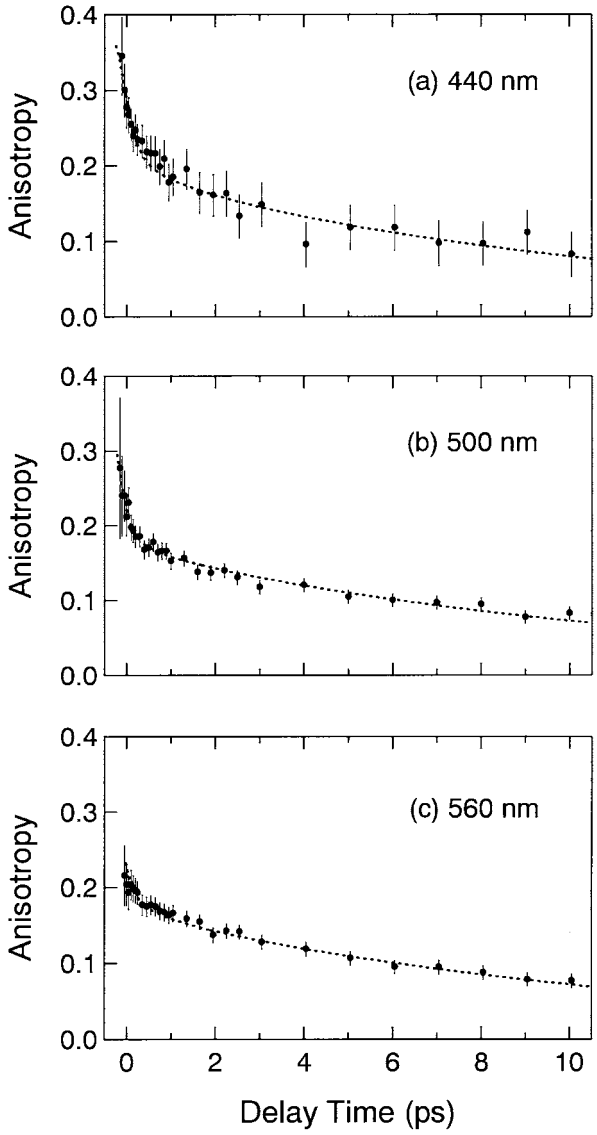

Figure 1. Time-resolved fluorescence anisotropy of 7-azaindole dimer in hexane measured at 440 (a), 500 (b), and 560 nm (c). Calculated anisotropy is also shown by a dotted curve.

VI-D-3 Investigation of Excited State Intramolecular Proton Transfer in Anthralin by Femtosecond Time-Resolved Fluorescence Spectroscopy

ARZHANTSEV, Sergei; TAKEUCHI, Satoshi; TAHARA, Tahei

Numerous elementary photoreactions in condensed phase occur on ultrafast time scale and femtosecond spectroscopy provides direct insight into the dynamics of such processes. The photoinduced intramolecular proton transfer of hydrogen-bonded molecules is a topic of current interest. Anthralin (1,8-dihydroxy-9(10H)-anthracenone) is of biological and pharmacological importance as antipsoriatic drug. Steady-state fluorescence excitation and emission spectra display an unusually large Stokes shift, indicating intramolecular proton transfer. The proposed scheme of photoinduced reaction is shown in Figure 1. Time-resolved fluorescence measurements were performed in a wide spectral

region from 480 nm to 690 nm. Several time-resolved fluorescence traces are presented in Figure 2. We observed the fast decays in blue side and coinciding fast rises in red side of the spectrum in (sub)picosecond time region, which gave us the information about the proton transfer rate. The global fit procedure was applied for quantitative analysis of experimental data. As results of fitting procedure, characteristic time constants (τ_1 = 0.1 ps, τ_2 = 1.4 ps, τ_3 = 120 ps) of excited state dynamics were obtained. The excited state dynamics were discussed in terms of excited-state intramolecular proton transfer and other pathways of the energy relaxation.

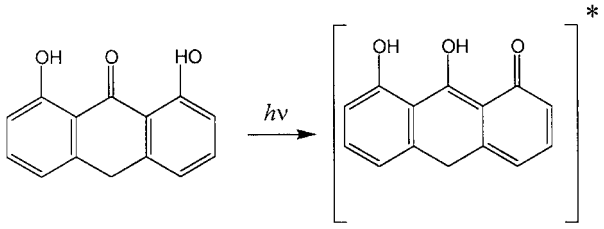

Figure 1. The proposed scheme of proton transfer in anthralin.

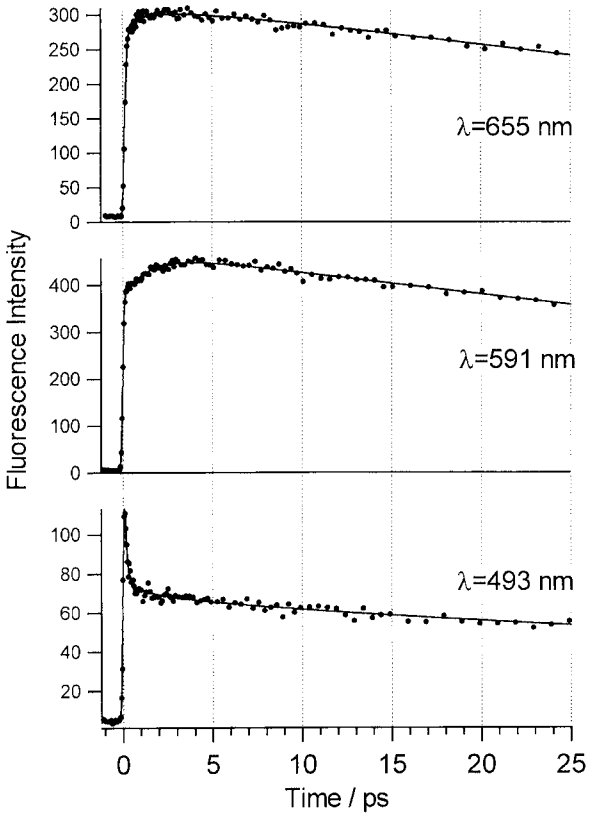

Figure 2. Time-resolved fluorescence traces obtained from anthralin at 655, 591 and 493 nm. The dots are experimental data and the solid curves are the results of the fitting analysis.

VI-D-4 Relaxation Kinetics of the S_n and S_1 States of Biphenyl Probed by Femtosecond Fluorescence Anisotropy

IWATA, Koichi[1]; TAKEUCHI, Satoshi; TAHARA, Tahei
([1]Univ. Tokyo)

Fluorescence intensity and its anisotropy decay of biphenyl were measured in hexane solution. The sample solution was photoexcited with a linearly polarized femtosecond light pulse at 270 nm. Time dependence of the fluorescence intensity as well as its anisotropy was measured with the up-conversion method. The observed fluorescence decay curve showed a fast decay component of 0.4 ps, in addition to a slow component corresponding to the reported fluorescence decay of 16 ns. The observed fluorescence anisotropy value at time 0 was approximately 0.4, indicating that the direction of the fluorescence transition dipole at time 0 is same as the S_n-S_0 absorption at 270 nm. The observed anisotropy change was well fitted by a double exponential decay function, with time constants of 0.2 ps and 9 ps. The fast component represents the S_n-S_1 internal conversion process, while the slow component corresponds to the rotational diffusion of the S_1 state. From the extrapolated value of the slow component at time 0, the angle between the effective transition dipoles of the S_n-S_0 transition and the S_1-S_0 transition was estimated to be 27 degrees.

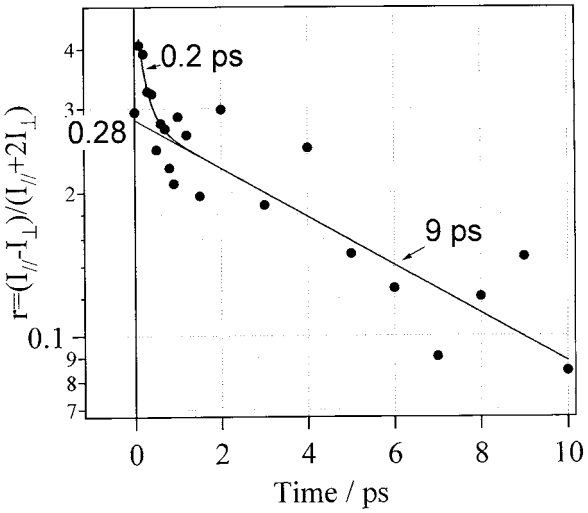

Figure 1. Time dependence of femtosecond fluorescence anisotropy of biphenyl.

VI-D-5 Lifetime Measurements of S_2 Emission from Zinc(II) Porphyrins by the Femtosecond Up-Conversion Method

ASANO-SOMEDA, Motoko[1]; ARZHANTSEV, Sergei; TAHARA, Tahei
([1]Tokyo Inst. Tech.)

In violation of Kasha's rule, upper excited-state emission has been observed for some polyatomic molecules. For instance, a variety of diamagnetic metalloporphyrins exhibit fluorescence from the secondary excited singlet (S_2) state even under the steady-state condition. Relatively intense S_2 emission of metalloporphyrins must be related with their characteristic electronic structure. In the typical diamagnetic metalloporphyrins, the S_1 and S_2 states are described as a 50-50 admixture of two common (π,π*) configurations, and this leads to almost parallel surfaces in the S_1 and S_2 states. In addition, there is a reasonably

large energy gap between the S_1 and S_2 states. Such features of metalloporphyrins slow $S_2 \rightarrow S_1$ internal conversion rates, thus allowing observation of S_2 emission.

Zinc(II) porphyrin is one of the typical diamagnetic metalloporphyrins and exhibits S_2 fluorescence. While subpicosecond lifetimes are estimated for such porphyrins from the quantum yields of S_2 emission, it is crucial to determine the lifetimes by means of time-resolved measurements. We have applied the femtosecond up-conversion method to a series of zinc(II) porphyrins. Figure 1 shows the decay of S_2 and rise of S_1 emission signals of TMPZn(II) (TMP denotes tetramesithylporphin) measured with 400 nm excitation. Both kinetic traces give the same time constant of 1.6 ps, which corresponds to the S_2 lifetime.

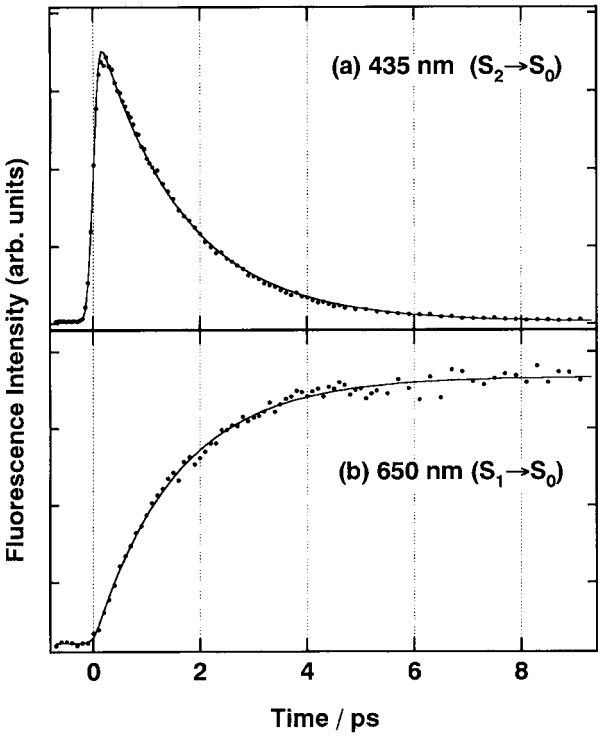

Figure 1. (a) Decay of S_2 and (b) rise of S_1 emission signals of TMPZn in toluene upon femtosecond laser irradiation at 400 nm. Experimental results are given by dots along with the best fitting curves in solid lines.

VI-D-6 Femtosecond Absorption Study on Ultrafast Decay Dynamics of Photoexcited Cu(II)(TMpy-P4) in Water Solvent

JEOUNG, Sae Chae; TAKEUCHI, Satoshi; TAHARA, Tahei; KIM, Dongho[1]
([1]KRISS)

[*Chem. Phys. Lett.* **309**, 369 (1999)]

Femtosecond time-resolved absorption spectroscopy was employed to investigate the relaxation dynamics of photoexcited copper(II) tetrakis(4-N-methylpyridyl)-porphyrin (Cu(II)(TMpy-P4)) in neat water. It was found that the transient absorption spectra as well as their temporal profiles exhibit a strong pump-power dependency, which is probably the cause of the discrepancy in the previous reports about dynamics of this molecule. It was concluded that the multiphoton ionization of solvent water takes place under the high pump-power condition. Time-resolved absorption spectra of Cu(II)(TMpy-P4) were measured with the pump power as low as 0.03 mJ/cm^2, and it was confirmed that the relaxation process finishes within 100 ps. We observed temporal changes of the excited-state(s) absorption in the picosecond region as well as the double exponential recovery of the ground state bleaching. The obtained time-resolved absorption data revealed that the relaxation process of photoexcited Cu(II)(TMpy-P4) in water is rather complicated and they suggested that several transient species (excited states) appear in the course of the relaxation. The relaxation mechanism of photoexcited Cu(II)(TMpy-P4) as well as the interaction with solvent water was discussed.

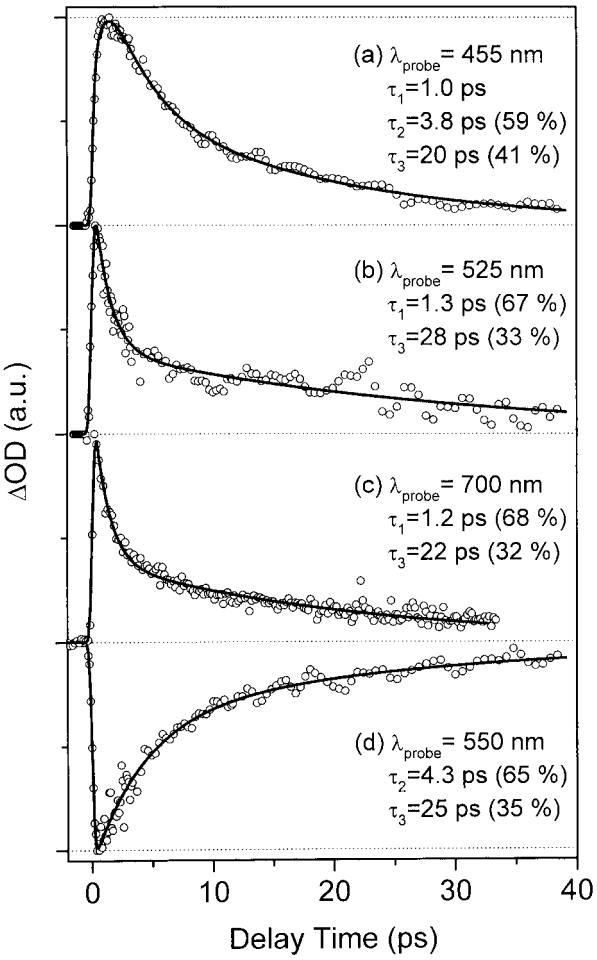

Figure 1. The time-resolved absorption changes of photo-excited Cu(II)(TMpy-P4) in water at three wavelengths of 455 (a), 525 (b) and 700 nm (c). The temporal change of the Q-band bleaching at 550 nm (d) was determined after correcting the baseline variation due to the photoinduced absorption.

VI-E Studies of Photochemical Reactions Using Picosecond Time-Resolved Vibrational Spectroscopy

Time-resolved vibrational spectroscopy is a very powerful tool for the study of chemical reactions. It often affords detailed information about the molecular structure of short-lived intermediates, which is not obtainable with time-resolved electronic spectroscopy. However, for molecules in the condensed phase, we need energy resolution as high as 10 cm^{-1} in order to obtain well-resolved vibrational spectra. This energy resolution is compatible only with time-resolution slower than picosecond because of the limitation of the uncertainty principle. In this sense, picosecond measurements are the best compromise between energy resolution and time resolution for time-resolved frequency-domain vibrational spectroscopy. In this project, we study photochemical processes and short-lived transient species by using picosecond time-resolved Raman spectroscopy. In this year, we focused on trans-azobenzene that is a prototypical molecule showing fast cis-trans isomerization. We studied the electronic and vibrational relaxation processes as well as the structure of the S_1 state of this molecule. In addition, while doing time-resolved Raman work, we recently noticed that amplified picosecond pulses are suitable for the excitation of hyper-Raman scattering.

VI-E-1 Picosecond Time-Resolved Raman Study of Trans-Azobenzene

FUJINO, Tatsuya; TAHARA, Tahei

[*J. Phys. Chem. A* in press]

The electronic and vibrational relaxation of photo-excited trans-azobenzene were investigated by pico-second time-resolved Raman spectroscopy. The second and third harmonic pulses of the regeneratively amplified output of a Ti:saphhire laser were used as the probe (410 nm) and the pump (273 nm). The frequency resolution of the measurement was approximately 10 cm^{-1} and time resolution was about 2 ps. With the 273-nm pumping pulse, the molecule is initially excited to the $S_2(\pi\pi^*)$ state, and the 410-nm probing wavelength is in resonance with the $S_n \leftarrow S_1$ transient absorption that appears in accordance with the decay of the S_2 state. Several transient Raman bands assignable to the S_1 state were observed immediately after photoexcitation. The lifetime of the S_1 state showed a significant solvent dependence and it was determined as ~12.5 ps in ethylene glycol and ~1 ps in hexane. Time-resolved anti-Stokes Raman measurements were also carried out for hexane solution to obtain information about vibrational relaxation process (Figure 1). We observed almost all S_1 Raman band in the anti-Stokes spectra, which implies that the S_1 state is highly vibrationally excited. In addition, several anti-Stokes Raman bands due to the S_0 state were observed after the decay of the S_1 state, indicating that the vibrationally excited S_0 azo-benzene was generated after electronic relaxation in hexane. The lifetime of vibrationally excited S_0 azo-benzene was evaluated as ~16 ps by the analysis for the intensity change of the anti-Stokes NN stretching band. The relaxation process of photoexcited *trans*-azo-benzene clarified in the present study is depicted in Figure 2.

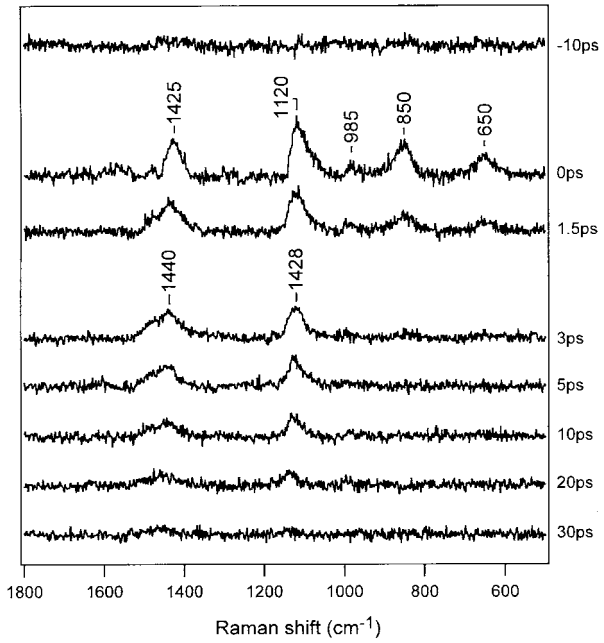

Figure 1. Picosecond time-resolved anti-Stokes Raman spectra of azobenzene in hexane in the delay time range from –10 ps to 30 ps (1.5×10^{-2} mol dm^{-3}; pump at 273 nm; probe at 410 nm).

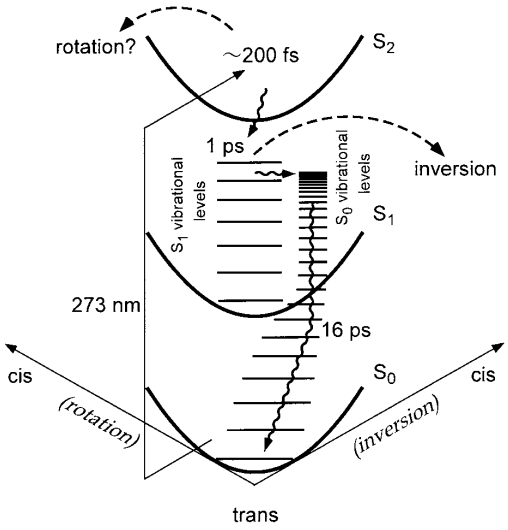

Figure 2. The relaxation mechanism of photoexcited trans-azobenzene (in hexane).

VI-E-2 Molecular Structure of S_1 Azobenzene: Vibrational Frequency of the NN Stretch Mode in the S_1 and S_0 State

FUJINO, Tatsuya; TAHARA, Tahei

Time-resolved vibrational spectra contain much information about the molecular structure of transient species. Concerning the S_1 state of azobenzene, information about the structure around the central NN bond is the most important because it can afford a clue to understand how the S_1 state participates in the photoisomerization process. In this sense, the assignment of the NN stretching vibration is crucial. We synthesized a ^{15}N-substituted analogue and measured S_1 Raman spectra in order to make unambiguous assignment about this key vibration and to discuss the molecular structure of the S_1 state.

Figure 1 shows transient Raman spectra of the normal species and the ^{15}N analogue ($(C_6H_6{}^{15}N)_2$) of the S_1 state of azobenzene. The spectra were measured for ethylene glycol solutions. The Raman spectra of the S_0 state are also shown in this figure for the comparison. In the S_1 spectra, it is clearly recognized that the Raman band at 1428 cm^{-1} shows a 27-cm^{-1} downshift with ^{15}N substitution. This S_1 band is straightforwardly attributable to the NN stretching vibration in the S_1 state. The NN stretching frequency in the S_1 state is almost same as that in the S_0 state (1440 cm^{-1}), which manifests that the NN bond in S_1 azobenzene retains a double bond character. The double bond nature of the NN bonding as well as high similarity in the spectral feature between S_1 Raman and S_0 Raman suggests that the observed S_1 azobenzene has a planar structure around the central NN bond.

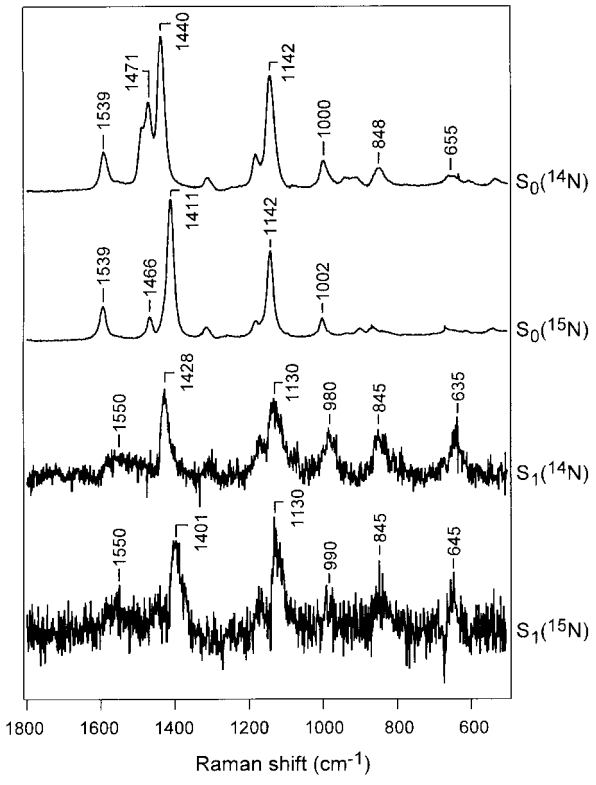

Figure 1. Raman spectra of azobenzene in the S_1 state and the S_0 state (in ethylene glycol). From the top to the bottom, normal species in the S_0 state, ^{15}N analogue in the S_0 state, normal species in the S_1 state, and ^{15}N analogue in the S_1 state. The S_1 spectra were taken at 0 ps. (1.5×10^{-2} mol dm^{-3}; pump at 273 nm; probe at 410 nm).

VI-E-3 Observation of Resonance Hyper-Raman Scattering of *all-trans* Retinal

MIZUNO, Misao; TAHARA, Tahei; HAMAGUCHI, Hiro-o[1]
([1]Univ. Tokyo)

High peak powered ultrafast lasers allow us to observe a variety of higher order optical processes. We recently found that a fairly strong hyper-Raman scattering of *all-trans* retinal can be observed by using the excitation with amplified picosecond pulses under a resonance condition, even from a diluted solution. A typical resonance hyper-Raman spectrum excited at 800 nm (ω) is shown in Figure 1(a). The probe pulse was the output of the picosecond regenerative amplifier of a Ti:sapphire laser system. The pulse width and the pulse energy were about 2 ps and 10 μJ, respectively. The resonance Raman spectrum excited at 400 nm (2ω) is shown in Figure 1(b), for comparison. The spectral pattern of the hyper-Raman and the Raman spectra is very similar to each other, although the intensity enhancement arises from two-photon resonance in hyper-Raman process while it is due to one-photon resonance in ordinary Raman. The similarity of these spectra suggests that resonance mechanism of hyper-Raman scattering is attributed to the A-term of the resonance hyper-Raman theory.[1)] We also measured resonance hyper-Raman spectra of *all-trans* retinal by probing at every 10 nm from 770 nm to 840 nm, and examined the excitation profiles.

Reference

1) Y. C. Chung and L. D. Ziegler, *J. Chem. Phys.* **88**, 7287 (1988).

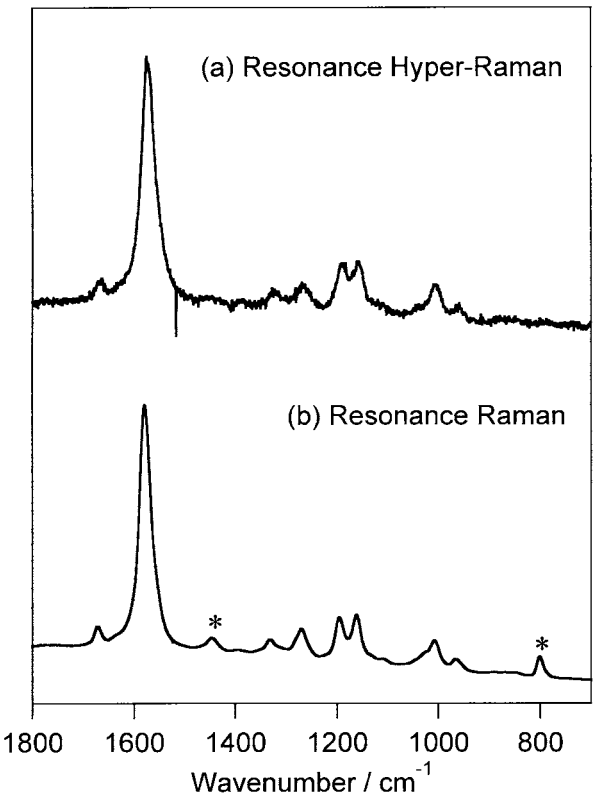

Figure 1. Comparison of (a) resonance hyper-Raman and (b) resonance Raman spectra of all-trans retinal in cyclohexane (1×10^{-3} mol dm^{-3}). Excitation wavelength is 800 nm for resonance hyper-Raman, and 400 nm for resonance Raman. The asterisks (*) indicate solvent bands.

VI-F Synchrotron Radiation Stimulated Surface Reactions

Study of synchrotron radiation (SR) stimulated surface reaction is a promising topic in fundamental science, because dynamical processes induced by the photostimulated coreelectron excitations on surfaces are scarcely explored so far. This field is important also in applied science, since the fundamental study is expected to develop the new techniques for semiconductor processing such as SR stimulated etching and SR stimulated epitaxial growth.

VI-F-1 Vibration Analysis of SiH_n Bending Modes on Hydrogenated Si(100) Surface Using Infrared Reflection Absorption Spectroscopy

NODA, Hideyuki; URISU, Tsuneo; HIRAMATSU, Mineo[1]
([1]Meijo Univ.)

Detailed analyses have been successfully made for the SiH_n stretching vibration mode on hydrogenated Si(100) surface, which is of great scientific and technological interest.[1)] However, concerning the bending vibration region, which gives important information about SiH_2 and SiH_3 species, very little work has been done. Recent developments of buried metal layer-infrared reflection absorption spectroscopy (BML-IRRAS) have made the high-resolution vibration analysis of the bending region easy. In this work, adsorption and desorption of hydrogen on Si(100) surfaces have been investigated by measuring BML-IRRAS covering a wide spectral range (800–2200 cm^{-1}). In both 3×1 and 1×1 phases observed with reflection high-energy electron diffraction (RHEED), a doublet peak (902 and 913 cm^{-1}) has been clearly observed and assigned to the SiH_2 scissors mode. The splitting of the peak is most likely due to the frequency difference of SiH_2 scissors vibration between single SiH_2 (ordered 3×1 units; H-Si-Si-H H-Si-H H-Si-Si-H) and neighboring SiH_2 (disordered 3×1 units; H-Si-Si-H H-Si-H H-Si-H H-Si-Si-H). Coverage and annealing temperature dependence of this doublet peak have also been investigated.

Reference

1) Y. J. Chabal and K. Raghavachari, *Phys. Rev. Lett.* **54**, 1055 (1985).

VI-F-2 Scanning Tunneling Microscopy for the Study of the Synchrotron-Radiation Stimulated Processes; Synchrotron-Radiation Stimulated Desorption of SiO_2 Films on Si(111) Surface

MIYAMAE, Takayuki; URISU, Tsuneo; UCHIDA, Hironaga[1]; MUNRO, Ian H.[2]
([1]Toyohashi Univ. Tech.; [2]UMIST)

[*Jpn. J. Appl. Phys.* **38**, 249 (1999)]

We have constructed a scanning tunneling microscopy (STM) system for the study of synchrotron radiation (SR) stimulated photochemical reactions. In order to eliminate the vibration and acoustic noise, the entire UHV chamber is mounted on a high-performance air-suspended vibration isolation table and was also covered by the soundproof mat. The mechanisms for SR stimulated desorption of SiO_2 thin films on the Si (111) surfaces have been investigated using the STM, low energy electron diffraction (LEED) , and Auger electron spectroscopy. An atomically flat and clean Si(111)-(7×7) surface was obtained after two hours SR irradiation at a surface temperature of 700 °C. The STM topograph suggests that the desorption mechanism may be completely different between thermal and SR stimulated desorption of SiO_2 film.

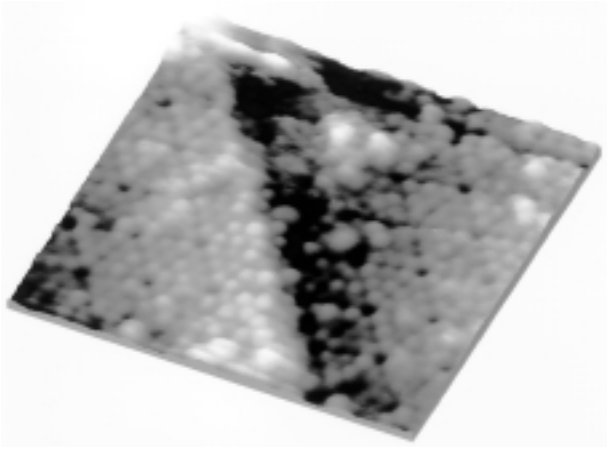

Figure 1. Three-dimensional STM image of 2 hours SR-irradiation to the samples at the sample temperature of 700 °C. Image size = 15 × 15 nm.

VI-F-3 Synchrotron-Radiation Stimulated Desorption of SiO_2 Thin Films on Si(111) Surfaces Observed by Scanning Tunneling Microscopy

MIYAMAE, Takayuki; UCHIDA, Hironaga[1]; MUNRO, Ian H.[2]; URISU, Tsuneo
([1]Toyohashi Univ. Tech.; [2]UMIST)

[*J. Vac. Sci. Technol., A* **17**, 1733 (1999)]

Synchrotron radiation (SR) stimulated desorption of silicon dioxide thin films was studied using scanning tunneling microscopy (STM) , low energy electron diffraction (LEED) , and Auger electron spectroscopy. Reconstructed Si(111)-7×7 patterns were observed by LEED after 2 h SR irradiation at a surface temperature of 700 °C. The STM images show an atomically flat Si(111)-(7×7) surface. STM topographs of SR-irradiated surfaces suggest that the oxide desorption mechanism is completely different from that of thermal desorption of SiO_2 film. These results indicate that the atomically flat Si surface can be obtained at low temperatures by using this technique.

VI-F-4 Direct Observation of Synchrotron Radiation Stimulated Desorption of Thin SiO_2 Films on Si (111) by Scanning Tunneling Microscopy

MIYAMAE, Takayuki; UCHIDA, Hironaga[1]; MUNRO, Ian H.[2]; URISU, Tsuneo
([1]Toyohashi Univ. Tech.; [2]UMIST)

[*Surf. Sci. Lett.* **437**, L755 (1999)]

This is the first report of the use of scanning tunneling microscopy (STM) to study changes in the surface morphology during synchrotron radiation (SR) stimulated desorption of SiO_2 films on Si(111). An atomically flat surface was obtained after two hours SR irradiation at a surface temperature of 700 °C. The STM topograph indicates that the SR desorption mechanism is quite different for the thermal desorption of SiO_2. The non-formation of multistep holes on the exposed Si surface indicates that the desorption of oxygen atoms and molecules by SR excitation leaving volatile SiO is an important mechanism.

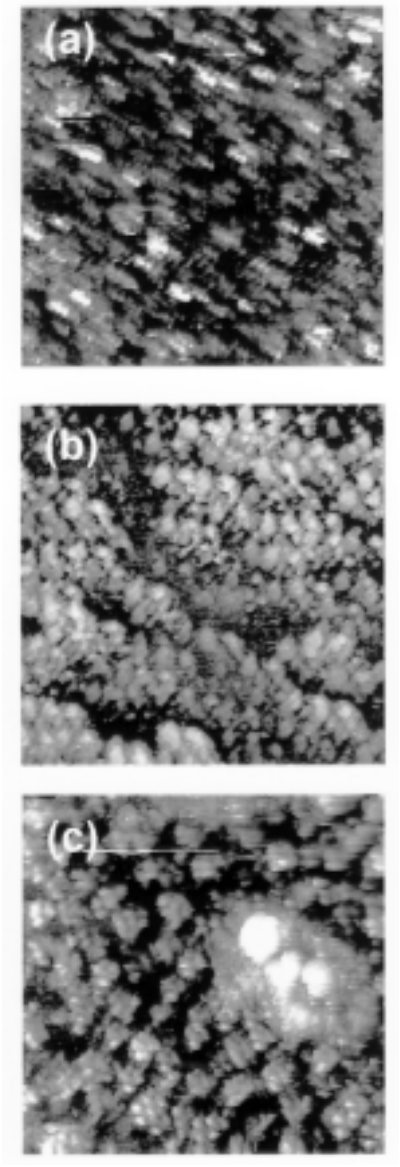

Figure 1. (a) STM image of Si (111) sample after 2.5 h SR-irradiation at the sample temperature of 650 °C. Image size = 2000 × 2000 Å. (b) STM image of 1 h SR-irradiation to the samples at the sample temperature of 700 °C. Image size = 5000 × 5000 Å. (c) STM image of 2 h SR-irradiation to the samples at the sample temperature of 700 °C.

VI-F-5 Scanning Tunneling Microscopy Study of Surface Morphology of Si(111) after Synchrotron Radiation Illumination

GAO, Yongli[1]; MEKARU, Harutaka; MIYAMAE, Takayuki[2]; URISU, Tsuneo
([1]Univ. Rochester; [2]Natl. Inst. Mater. Chem. Res.)

The surface morphology of Si(111) was investigated using scanning tunneling microscopy the after illumination by synchrotron radiation. The surface shows large regions of atomically flat Si(111)-7×7 structure, and is characterized by the formation of bilayer atomic steps nicely registered to the crystal structure. The pinning of the steps by nanometer scale dust sis evident. This is in sharp contrast to Si(111) surfaces after thermal desorption of SiO_2 at temperatures 880 °C and above, where the surface steps are much more irregular. The registration of the surface steps to the underlying crystal structure indicates that the bilayer atomic steps reach thermodynamic equilibrium under synchrotron radiation at temperatures much lower than that necessary for thermal desorption.

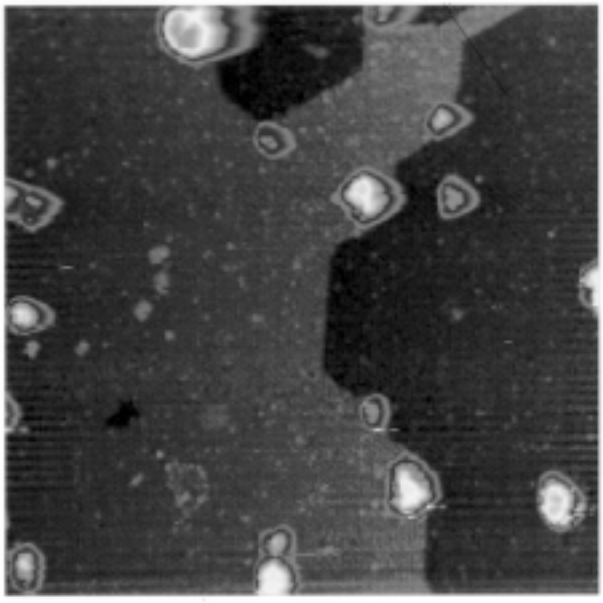

Figure 1. 1000 × 1000 $Å^2$ topograph of a Si(111) surface after 5 hours of SR irradiation at 650 °C. The most striking feature of the topography is the bilayer steps in alignment to the high symmetry axes of the surface.

VI-F-6 Construction of the Multilayered-mirror Monochromator Beam Line for the Study of Synchrotron Radiation Stimulated Process

MEKARU, Harutaka; TSUSAKA, Yoshiyuki[1]; MIYAMAE, Takayuki; KINOSHITA, Toyohiko; URISU, Tsuneo; MASUI, Shin[2]; TOYOTA, Eijiro[2];

TAKENAKA, Hisataka[3]
([1]Himeji Inst. Tech.: [2]Sumitomo Heavy Ind. Ltd.; [3]NTT-AT)

[*Rev. Sci. Instrum.* **70**, 2601 (1999)]

A multilayered-mirror (MLM) monochromator beam line designed specially for synchrotron radiation (SR) stimulated process experiments has been constructed for the first time. The beam line was designed by the criteria ; a beam spot size on the sample surface ≥ 3 × 3 mm^2, a density of total irradiated photons ≥ 10^{18} photons/cm^2 (for an irradiation time of a few tens of minutes to a few hours) and low-energy background ≤ 1% of the output. The performance of the beam line was evaluated by measuring the transmitted photon flux of an Al filter around the Al $L_{2,3}$ absorption edge and by measuring the photo-emission spectra of Ta using the output beam as an excitation light source. The Al thin film deposition was successfully demonstrated by using the monochromatized output beam. We conclude that this MLM monochromator performs sufficiently well to study the excitation energy dependence in SR-stimulated processes.

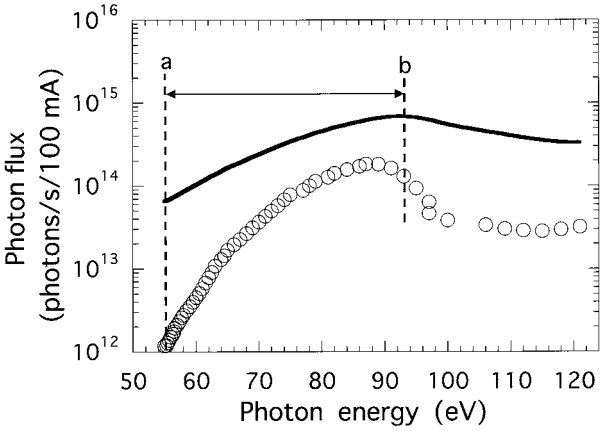

Figure 1. The dependence on the photon energy of the photon flux of output beam. The solid line shows calculated values and "○" shows measured values. The dotted lines a and b show the working region of the monochromator.

VI-F-7 Excitation Energy Dependence on Composition of an Al Deposited-thin Film Stimulated by Monochromatized SR

MEKARU, Harutaka; URISU, Tsuneo

The output beam of a multilayered-mirror monochromator beam line (BL4A1) at the UVSOR of the IMS was applied to an Al thin film deposition using dimethylaluminum hydride (DMAH) low temperature condensed layer. After cooling Si(100) substrate to about 100 K, the DMAH gas was introduced and deposited on the substrate (10–20 monolayers). The surface of the substrate was irradiated by the monochromatized SR beam tuned to the Al 2p core electron excitation energy, and the composition of the deposited film was measured by XPS at room temperature. An interesting point is the C concentration of the deposited film. By assuming C/Al = 2 for DMAH condensed layer before irradiation, the minimum composition C/Al of the deposited film is estimated to be about 0.65. This value is quite small compared with those of films obtained by the white or filtered white SR beams irradiations. This may be due to that the Al-C bond is preferentially broken by the Al core electron excitations.

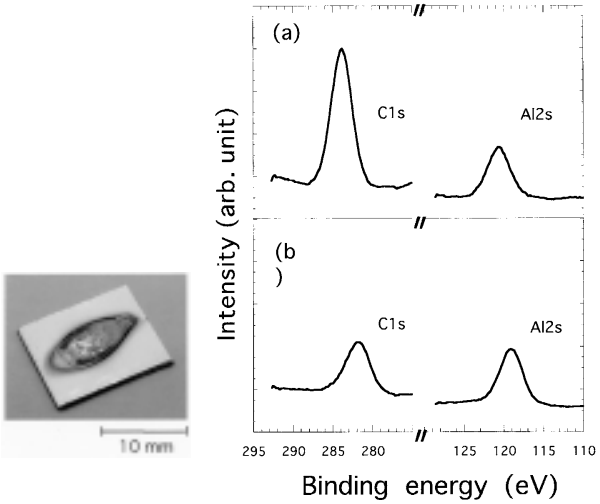

Figure 1. Photograph of the deposited Al thin film and the observed XPS spectra for (a) the DMAH condensed layers at 105 K and (b) the deposited Al thin film.

VI-F-8 SR-stimulated Etching and OMVPE Growth for Semiconductor Nano-structure Fabrication

NONOGAKI, Youichi[1]; HATATE, Hitoshi[1]; OGA, Ryo[1]; YAMAMOTO, Shunsuke[1]; FUJIWARA, Yasufumi[1]; TAKEDA, Yoshikazu[1]; NODA, Hideyuki; URISU, Tsuneo
([1]Nagoya Univ.)

We proposed a new method to form ordered array of the quantum dots using SR-stimulated etching and selective area growth by OMVPE. The SR etching has a great potential for fabrication of semiconductor devices, because side wall is very vertical and the induced damage of the etched surface is extremely low. Neither of them can be achieved by wet chemical etching or RIE. We report here preliminary results on SR etching of SiO_2 on InP substrate and growth of InP on the patterned substrate. SR etching was performed by exposing SiO_2 to SR irradiation in SF_6 ambient. The etched depth dependence on SF_6 pressure ranging from 5×10^{-8} Torr to 0.5 Torr was investigated at SR irradiation dose of 10,000 mA·min. The maximum etching rate in this study was 4.7×10^{-3} nm/(mA·min) at SF_6 pressure of 0.05 Torr. Using the SR etching, we patterned SiO_2 with 0.4 μm opening on the InP substrate. Selective area growth of InP was successfully observed on the patterned substrate. In the low-temperature PL measurement, exciton related emission lines were clearly observed.

VI-G Ion Desorption Induced by Core-Electron Transitions Studied by Electron Ion Coincidence Spectroscopy Combined with Synchrotron Radiation

Ion Desorption Induced by Core-Electron Transitions has been studied using energy-selected electron ion coincidence spectroscopy combined with synchrotron radiation. Auger electron photo-ion coincidence (AEPICO) and photoelectron photo-ion coincidence (PEPICO) spectroscopy proved to be an ideal tool for investigations of the ion desorption induced by core-level excitations. AEPICO results show that the character of the orbitals where holes are created, as well as the effective hole-hole Coulomb repulsion are important factors in the Auger-stimulated ion desorption from covalent molecules. The PEPICO spectroscopy, on the other hand, provided direct evidences of site-specific ion fragmentation induced by core-level excitations.

VI-G-1 Study of Ion Desorption Induced by a Resonant Core-Electron Transition of Condensed H_2O by Using Auger Electron Photoion Coincidence (AEPICO) Spectroscopy Combined with Synchrotron Radiation

MASE, Kazuhiko; NAGASONO, Mitsuru; TANAKA, Shin-ichiro; URISU, Tsuneo; IKENAGA, Eiji; SEKITANI, Tetsuji; TANAKA, Kenichiro[1]
([1]Hiroshima Univ.)

Proton desorption mechanism in the region of resonant excitations of Oxygen 1*s* core-electron of condensed water is studied using Auger electron photoion coincidence (AEPICO) spectrometer with an improved resolution of the electron kinetic energy of $E/\Delta E$ = 100. The spectrum of total ion yield divided by Auger electron yield (AEY, electron kinetic energy: 490 eV) exhibited a characteristic threshold peak at the $4a_1 \leftarrow$ O:1*s* resonance ($h\nu$ = 532.3 eV) and a suppression at the $3p \leftarrow$ O:1*s* resonance ($h\nu$ = 535.5 eV). The electron kinetic energy dependence of the AEPICO yield (AEPICO yield spectra) were measured at $h\nu$ = 532.6, 533.6, 335.4, 540.6, 547.6 and 557.8 eV. At the $4a_1 \leftarrow$ O:1*s* resonance ($h\nu$ = 532.6 eV) and $2b_2 \leftarrow$ O:1*s* resonance ($h\nu$ = 533.6 eV), the AEPICO yield spectrum exhibited major, medium and minor peaks at the electron kinetic energies of 502.5, 485 and 465 eV, which are assigned to $(\mathrm{O}{:}2p)^{-2}(4a_1 \text{ (or } 2b_2))^1$, $(\mathrm{O}{:}2s)^{-1}(\mathrm{O}{:}2p)^{-1}(4a_1 \text{ (or } 2b_2))^1$, and $(\mathrm{O}{:}2s)^{-2}(4a_1 \text{ (or } 2b_2))^1$ spectator Auger final states, respectively. These results shows that ultrafast ion desorption (UFID) mechanism is predominant at the $4a_1$ and $2b_2$ resonances. The enhancement of the H^+ AEPICO yield was attributed to the strongly O-H antibonding character of $4a_1$ and $2b_2$ orbitals. At the 3*p* resonance ($h\nu$ = 535.4 eV), the AEPICO yield spectrum exhibited major, medium and minor peaks at the electron kinetic energies of 460, 475 and 490 eV, which are assigned to $(2a_1)^{-2}(3p)^1$, $(2a^1)^{-1}(1b_2)^{-1}(3p)^1$, and $(1b_2)^{-2}(3p)^1$ spectator Auger final states, respectively. This result indicates that spectator Auger stimulated ion desorption (SASID) mechanism is responsible at the 3*p* resonance. The suppression of the H^+ AEPICO yield was attributed to the reduction of the hole-hole Coulomb repulsion due to the 3*p* electron. At $h\nu$ = 540.6, 547.6 and 557.8 eV, the AEPICO yield spectrum exhibited three peaks at the electron kinetic energy of 460, 475 and 490 eV, which are assigned to $(2a_1)^{-2}$, $(2a_1)^{-1}(1b_2)^{-1}$, and $(1b_2)^{-2}$ normal Auger final states, respectively. This result indicates that the normal Auger stimulated ion desorption mechanism is responsible at photon energies above the O:1*s* ionization. These results and conclusions are consistent with the previous study carried out by low-resolution AEPICO spectroscopy.[1)]

Reference
1) K. Mase, *et al.*, *J. Chem. Phys.* **108**, 6550 (1998).

VI-H Photoionization Dynamics Studied by Electron Spectroscopy Combined with a Continuous Synchrotron Radiation Source

Molecular photoionization is a major phenomenon in vacuum UV excitation and provides a large amount of information on fundamental electron-core interactions in molecules. Especially, neutral resonance states become of main interest, since they often dominate photoabsorption cross sections and lead to various vibronic states which are inaccessible in direct ionization. We have developed a versatile machine for photoelectron spectroscopy in order to elucidate dynamical aspects of superexcited states such as autoionization, resonance Auger decay, predissociation, vibronic couplings, and internal conversion. Introduction of a new methodology, two-dimensional photoelectron spectroscopy, allows us to investigate superexcited states in the valence excitation region of acetylene, nitric oxide, carbonyl sulfide, sulfur dioxide and so on. In this method, the photoelectron yield is measured as a function of both photon energy and electron kinetic energy (binding energy). The spectrum, usually represented as a contour plot, contains rich information on photoionization dynamics.

VI-H-1 Autoionization of a Dipole-Forbidden Superexcited State of CS_2

MITSUKE, Koichiro; HIKOSAKA, Yasumasa[1]
([1]Inst. Mater. Struct. Sci.)

Two-dimensional photoelectron spectroscopy of CS_2 has been employed to study excitation and autoionization mechanism of Rydberg states with the aid of analyses of the vibrational branching ratios of the final ions. The photoelectron yield is measured as a function of both photon energy $E_{h\nu}$ and ionization energy I_E. Figure 1 shows a spectrum in the $E_{h\nu}$ range of 14.6-15.3 eV. The Rydberg state at $E_{h\nu}$ = 14.88 eV shows anomalously intense patterns at I_E =10.23 and 10.28 eV, which are identified as the v_3 = 1 vibrational levels of the antisymmetric stretching mode v_3 of the two spin-orbit components of CS_2^+ [$(2\pi_g)^{-1}$ X $^2\Sigma_{g,\Omega}$, Ω = 1/2 and 3/2]. Similar enhancement of the v_3 = 1 level has been also observed for autoionization of the Rydberg state at 14.88 eV to CS_2^+ [$(5\sigma_u)^{-1}$ B $^2\Sigma_u^+$]. This Rydberg state is considered to be the v_3 = 1 level of the $(6\sigma_g)^{-1}(3d\sigma_g)^1$ $^2\Sigma_g^+$ state converging to CS_2^+ [$(6\sigma_g)^{-1}$ C $^2\Sigma_g^+$]. The electronic dipole transition is forbidden from the ground state CS_2 (X $^1\Sigma_g^+$) to this Rydberg state, but comes to have a substantial oscillator strength through vibronic coupling involving the v_3 vibration. Conceivably, the transition to the $(6\sigma_g)^{-1}(3d\sigma_g)^1$ $^2\Sigma_g^+$, v_3 = 1 vibronic state borrows the intensity from a nearby dipole-allowed transition. From a broad line profile and a shift in the quantum defect, we conclude that the intensity is borrowed from the transition to the vibrational ground state of $(6\sigma_g)^{-1}(5p\sigma_u)^1$ $^2\Sigma_u^+$ observed at $E_{h\nu}$ = 14.951 eV.

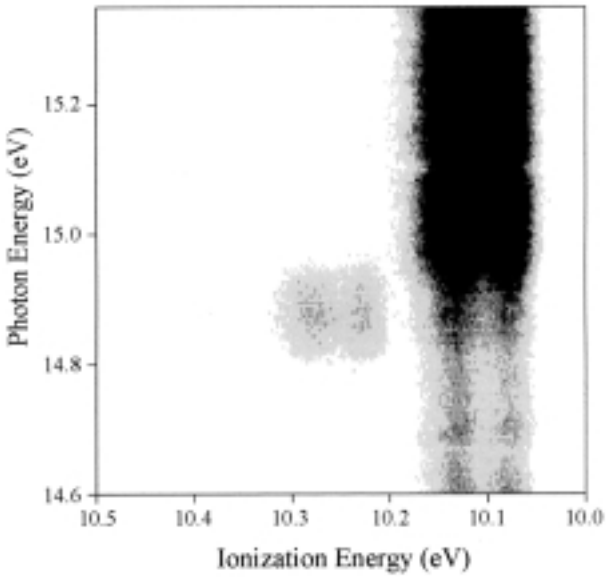

Figure 1. First band in the two-dimensional photoelectron spectrum of CS_2 corresponding to the formation of CS_2^+ (X $^2\Pi_{g,1/2}$, $^2\Pi_{g,3/2}$). The electron intensity is plotted with eight tones from light to dark on a linear scale. The photon wavelength resolution is 0.8 Å (15 meV at $E_{h\nu}$ = 15 eV) and the overall electron energy resolution is set to 40 meV.

VI-I Laser Photionization of Polarized Atoms Produced by Excitation with Synchrotron Radiation

In conventional photoionization experiments, the most standard method has generally been taken to be measurement of energy and angular distributions of photoelectrons from randomly oriented (unpolarized) atoms or molecules. However, information obtained from these experiments is insufficient, since the initial state constituted of atoms and photons is not selected and the internal properties of final photoions and electrons are not analyzed. In this project, we have performed photoelectron spectroscopy of polarized atoms using linearly-polarized laser light, aiming at complete quantum-mechanical photoionization experiments. Initial excitation with a linearly polarized synchrotron radiation permits ensemble of atoms to be aligned along the electric vector of the light. From an angular distribution of photoelectrons from polarized atoms, we are able to gain insight into the magnitude and phase shift difference of transition dipole matrix elements of all final channels which are allowed by selection rules.

VI-I-1 Laser Photoionization Electron Spectroscopy of Polarized Rare Gas Atoms Excited with Synchrotron Radiation

IWASAKI, Kota; HIKOSAKA, Yasumasa[1]; MITSUKE, Koichiro
([1]Inst. Mater. Struct. Sci.)

Laser photoionization processes of polarized rare gas atoms have been observed in order to study spin-orbit interactions of many electron systems and exploit the possibility of the complete photoionization experiment. Photoelectrons emitted in the direction perpendicular to both the laser and synchrotron radiation are detected with a 160° spherical electrostatic analyzer. In Figure 1(a), the photoelectron yield for $Ar(5s'[1/2]_1) \rightarrow Ar^+(^2P_{1/2}) + e^-$ (l = 1; j = 1/2, 3/2) is plotted as a function of the angle φ_e between the electric vector of the laser and the direction of the linear momentum of photoelectrons. The angular distribution should be interpreted in terms of a p partial wave from excited Ar atoms aligned toward the electric vector of synchrotron radiation.We have obtained an asymmetry parameter β of 1.7 ± 0.2 from Figure 1(a). The angular distributions have also been measured for photoelectrons produced by the process $Ar(3d[1/2]_1) \rightarrow Ar^+(^2P_{J_f}) + e^-$ (l = 1 or 3; j = 1/2, 3/2 or 5/2, 7/2) with J_f = 1/2 and 3/2 as illustrated in Figure 1(b). Here, J_f is the total angular momentum quantum number of Ar^+. The β values for these distribution curves were found to be 0.64 ± 0.04 and 0.90 ± 0.07 for the J_f = 3/2 and 1/2 states of Ar^+, respectively. We are planning to perform the complete photoionization experiment to determine dipole matrix elements and phase shift differences for all final open channels.

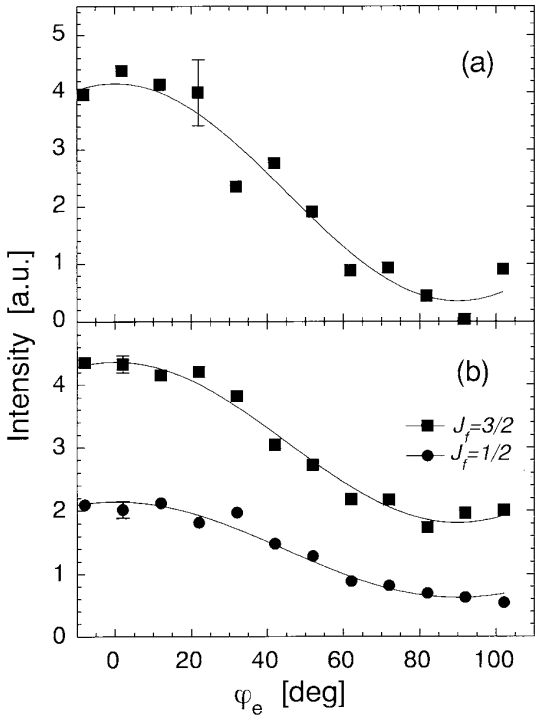

Figure 1. Angular distributions of photoelectrons: (a) $Ar(5s'[1/2]_1) \rightarrow Ar^+(^2P_{1/2}) + e^-$ (l = 1; j = 1/2, 3/2), (b) $Ar(3d[1/2]_1) \rightarrow Ar^+(^2P_{1/2,3/2}) + e^-$ (l = 1 or 3; j = 1/2, 3/2 or 5/2, 7/2) .

VI-I-2 Theoretical Angular Distribution of Photoelectrons from Polarized Ar Atoms

MITSUKE, Koichiro; HIKOSAKA, Yasumasa[1]; IWASAKI, Kota
([1]Inst. Mater. Struct. Sci.)

The photoelectron angular distribution of Ar Rydberg atoms produced by excitation with linearly polarized synchrotron radiation is given under the present experimental geometry by

$$\frac{d\sigma}{d\Omega} = \frac{\sigma^{(iso)}}{4\pi}\left[1 + \sqrt{\frac{5}{3}}\overline{A_{20}}\beta_{220} - \left(\sqrt{\frac{5}{6}}\beta_{022} + \sqrt{\frac{5}{6}}\overline{A_{20}}\beta_{202} - \frac{5}{\sqrt{21}}\overline{A_{20}}\beta_{222} + \sqrt{\frac{15}{7}}\overline{A_{20}}\beta_{242}\right) \times \frac{1}{2}(1 + 3\cos 2\varphi_e)\right]$$

where the normalized statistical tensor of the initial state $\bar{A}_{20}$ is proportional to the zero component of the statistical tensor in a coordinate frame with the z-axis directed along the symmetry axis for the pumping process producing the polarized atoms. We have derived the expression[1)] which connects generalized asymmetric coefficients $\beta_{k_0kk_\gamma}$ for the angular distribution with theoretical dynamic parameters involving reduced forms of transition dipole matrix elements, $\exp(i\delta_{l,j})\langle \varepsilon\, l; J \| D \| n_0\, l_0\rangle$. Here, J is the total angular momentum quantum number of the final state. In the case of photoionization of $Ar(5s'[1/2]_1)$, accessible open channels are four, which are designated as (j, J) = (1/2, 0), (1/2, 1), (3/2, 1), and (3/2, 2). Hence, the number of independent theoretical dynamic parameters is seven: four reduced dipole matrix elements, $D_{jJ} = \langle \varepsilon, l = 1, j; J \| D \| n_0 = 5,\ l_0 = 0\rangle$, and three phase shift differences, $\delta_{l=1,jJ} - \delta_{l=1,j'J'}$. The anisotropy of the observed angular distribution can be reasonably explained, assuming that the matrix elements and phase shift differences are essentially independent of J and that the spin-orbit interaction in the continuous spectrum is small.

Reference

1) K. Mitsuke, Y. Hikosaka and K. Iwasaki, *J. Phys. B* submitted.

VI-J Vacuum UV Spectroscopy Making Use of a Combination of Synchrotron Radiation and a Mode-Locked or Pulsed UV Laser

An ultraviolet laser system has been developed which synchronizes precisely with the synchrotron radiation (SR) from the storage ring of the UVSOR facility. A mode-locked Ti:sapphire laser is made to oscillate at the frequency of the ring in a multibunch operation mode. The delay timing between SR and laser pulses can be changed from 0 to 11 ns. We have developed another system, a pulsed dye laser pumped by an excimer laser, for SR-laser combination experiments. The second harmonic of the dye laser is tunable at 265–280 nm with a pulse energy of *ca.* 2 mJ pulse^{-1} at a repetition rate of 10–100 Hz. This laser system is mainly devoted to observing neutral species produced by neutral or ionic photofragmentation induced by SR excitation of molecules. The following three combination studies have been performed: (1) two-photon ionization of helium atoms studied as the prototype of the time-resolved experiment, (2) laser induced fluorescence (LIF) excitation spectroscopy of $N_2^+(X\ ^2\Sigma_g^+)$ ions produced by synchrotron radiation photoionization of N_2 or N_2O, and (3) resonance enhanced multiphoton ionization (REMPI) spectroscopy of $S(3s^2 3p^4\ ^3P_{J''}, J'' = 0, 2)$ dissociated from Rydberg states of OCS. Among these topics LIF spectroscopy of ions is making marked progress in improvements of spectral resolution and fluorescence counts. These improvements are brought about by introducing an RF ion trap and by narrowing the laser band-width. As a consequence, we can obtain reliable rotational distribution curves of $N_2^+(X\ ^2\Sigma_g^+)$.

VI-J-1 Improvement in the Energy Resolution of Laser Induced Fluorescence Excitation Spectroscopy of Ionic Species Produced by SR Photoexcitation

NIIKURA, Hiromichi[1]; MIZUTANI, Masakazu; MITSUKE, Koichiro
([1]GUAS)

Pump-probe spectroscopy making use of a combination of laser and synchrotron radiation has been performed at the beam line BL3A2 in UVSOR to study ionization and dissociation dynamics in the vacuum UV energy region. The fundamental light emitted from the planar-type undulator was dispersed by a 2.2 m grazing incidence constant deviation monochromator in the photon energy range 15.5–19 eV. The second harmonic of a mode-locked Ti:sapphire laser was used to probe cations produced by SR photoionization. Fluorescence was collected in the perpendicular direction to the two light beams and dispersed by another monochromator and detected with a photomultiplier tube. To increase the number density of ions, we employed a cylindrical ion trap, in which collisional quenching of the rotational distribution of ions can be disregarded. Figure 1 shows an LIF spectrum of $N_2^+(X\ ^2\Sigma_g^+, v = 0, N)$ produced by the photoexcitation of N_2 at the SR photon energy of 15.983 eV. This energy is equal to the excitation energy for the formation of the $4d\sigma_g\ ^1\Pi_u$ Rydberg state converging to N_2^+ $(A\ ^2\Pi_u, v = 0)$. We can clearly resolve the rotational structures of the *R*-branch resulting from the transition of N_2^+ $(B\ ^2\Sigma_u^+, v = 0, N + 1) \leftarrow (X\ ^2\Sigma_g^+, v = 0, N)$. The spectral resolution of 1.6 cm^{-1} (0.2 meV) has been achieved.

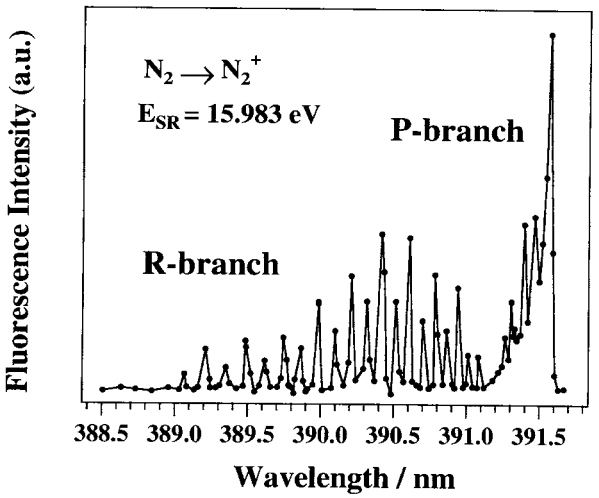

Figure 1. LIF excitation spectrum of the $(B\ ^2\Sigma_u^+, v = 0, N') \leftarrow (X\ ^2\Sigma_g^+, v = 0, N'')$ transition of N_2^+ produced by SR photoionization of N_2.

VI-J-2 Rotational State Distribution of N_2^+ Produced from N_2O

NIIKURA, Hiromichi[1]; MIZUTANI, Masakazu; MITSUKE, Koichiro
([1]GUAS)

We have measured LIF spectra of $N_2^+(X\ ^2\Sigma_g^+, v = 0, N)$ produced by SR excitation of N_2O. The spectral resolution of the probing laser was set to 11 cm^{-1}. Figure 1 shows an LIF spectrum of N_2^+ obtained at the photon energy of 18.556 eV, which value accords with the excitation energy for the formation of the $3d\pi$ Rydberg state converging to $N_2O^+(C\ ^2\Sigma)$. Auto-ionization to the vibrational manifolds of $N_2O^+(B\ ^2\Pi)$ is followed by the dissociation into $N_2^+(X\ ^2\Sigma_g^+) + O(^3P^e)$. Two maxima centered at 391.54 and 390.8 nm are ascribed to the *P* and *R* branches, respectively, for the $(B\ ^2\Sigma_u^+, v = 0, N') \leftarrow (X\ ^2\Sigma_g^+, v = 0, N'')$ transition. The rotational temperature of N_2^+ is estimated to be 200–230 K by fitting observed data points with the

theoretical intensity distribution with changing the temperature as a parameter. For the purpose of comparison, the average rotational energy of the $N_2^+(X\ ^2\Sigma_g^+)$ fragment was calculated as a function of the ∠NNO angle on the basis of the *modified impulsive model*. We assumed a stiff NN bond and no vibrational excitation of the N_2^+ fragment. This analysis suggests that the ∠NNO angle of $N_2O^+(B\ ^2\Pi)$ in the equilibrium geometry is larger than 160°.

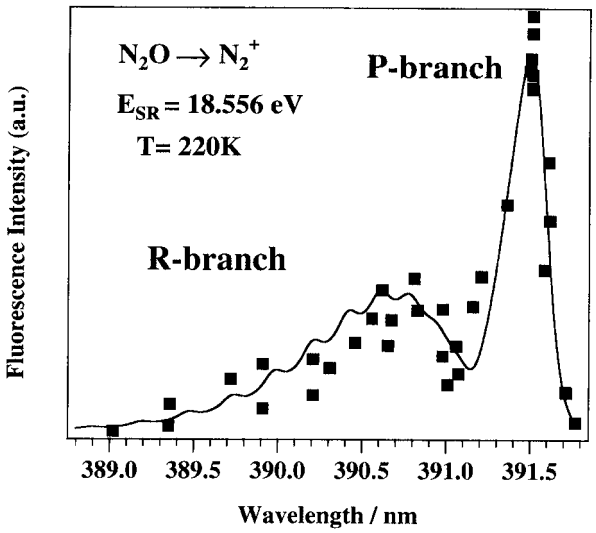

Figure 1. LIF spectrum of the ($B\ ^2\Sigma_u^+$, v = 0, N') ← ($X\ ^2\Sigma_g^+$, v = 0, N") transition of N_2^+ produced by SR photoionization of N_2O. The soild line represents the calculated rotational distribution at the temperature of 220 K.

VI-K Monochromator Newly Developed on the Beam Line BL2B2 in UVSOR

A grazing incidence monochromator has been constructed which supplies photons in the energy region from 20 to 200 eV. This monochromator will bridge the energy gap between the beam lines BL3A2 and BL8B1, thus providing for an accelerating demand for the high-resolution and high-flux photon beam from the research field of photoexcitation of inner-valence electrons or *L*-shell electrons in the third-row atom.

VI-K-1 First Performance Test of the 18 m-Spherical Grating Monochromator

ONO, Masaki; HATTORI, Hideo; YOSHIDA, Hiroaki[1]; MITSUKE, Koichiro
([1]Hiroshima Univ.)

This monochromator of Dragon type has been designed to cover the energy range of 20-200 eV with three gratings (G1, 80-200 eV; G2, 40-100 eV; G3, 20-50 eV). The resolving power ($E/\Delta E$) of 5000 and the photon flux of more than 1×10^{10} photons s^{-1} are expected at a 100 mA ring current.[1)] The performance is now being examined by measuring photoionization efficiency curves of rare gas samples introduced into a differentially pumped chamber at the end station.

Figure 1 shows a He^+ efficiency curve in the region of the $2snp \pm 2pns$ series resulting from doubly excited of He. The widths of the entrance and exit slits of the monochromator were set to 50 μm. The members up to n = 14+ of the series are clearly observed. The spectral width of the 14+ line is about 6.5 meV (FWHM). We therefore evaluate that $E/\Delta E$ of approximately 10^4 has been achieved at 65 eV. When $E/\Delta E$ is lowered to 6500 by changing the slit widths to 100 μm, the photon flux at 65 eV is estimated to be 1×10^{10} photons s^{-1}. Next, the photon energy is tuned at 91.2 eV which agrees with the excitation energy of the $5p \leftarrow 3d_{5/2}\ 5p[3/2]_1$ state of Kr. From the band width of its resonance peak, $E/\Delta E$ is estimated to be 4500 with the slit widths of 50 μm.

Reference
1) H. Yoshida and K. Mitsuke, *J. Synchrotron Radiat.* **5**, 774 (1998).

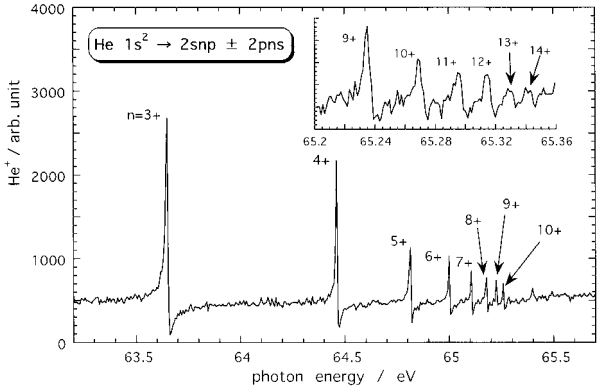

Figure 1. Photoionization efficiency curve exhibiting the $2snp \pm 2pns$ series of the doubly-excited He atom measured with the slit widths of 50 μm. Inset shows an enlarged spectrum in the region of $n \geq 9+$.

VI-L Ultraviolet Photoelectron Spectroscopy on Organic Thin Films Using Synchrotron Radiation

The electronic structure and molecular orientation of organic thin films were investigated by angle-resolved UPS with synchrotron radiation. Furthermore corresponding spectroscopies, such as low energy electron transmission spectroscopy, electron energy loss spectroscopy and Penning ionization electron spectroscopy were used in investigating the electronic states of the thin films.

VI-L-1 Origin of Photoemission Intensity Oscillation of C_{60}

HASEGAWA, Shinji; MIYAMAE, Takayuki; YAKUSHI, Kyuya; INOKUCHI, Hiroo; SEKI, Kazuhiko[1]; UENO, Nobuo
([1]Nagoya Univ.)

The photon-energy dependences of photoemission intensities of C_{60} were quantitatively calculated by the single-scattering approximation for the final state and the ab initio molecular orbital calculation for the initial state. The calculated results agreed well with the measured intenslty oscillation in the photon-energy range of $h\nu$ = 18–110 eV. The calculation by the plane-wave approximation for the final state also gave similar oscillations, which suggests that the oscillations are independent of the accuracy of the final state. These results indicated that the oscillations originate from the interference of photoelectron waves emanating from the 60 carbon atoms, *i.e.*, the multicentered photoemission with the phase difference of each wave. Further, the analytical calculation with a simplified spherical shell-like initial state revealed that the sphelcal structure of C_{60} molecule and its large radius dominate the oscillations.

VI-L-2 Pennìng Ionization Electron Spectroscopy on Self-Assembled Monolayer of 1-Mercapto-8-Bromooctane on Au(111)

ABDUREYIM, Abduaini[1]; KERA, Satoshi[1]; SETOYAMA, Hiroyuki[1]; SUZUKI, Ryouichi[2]; AOKI, Masaru[2]; MASUDA, Shigeru[2]; OKUDAIRA, Koji K.[1]; YAMAMOTO, Makoto[1]; UENO, Nobuo; HARADA, Yoshiya[1]
([1]Chiba Univ., [2]Univ. Tokyo)

Penning ionization electron spectroscopy (PIES) and ultraviolet photoelectron spectroscopy (UPS) were used to charactenze self-assembled monolayers (SAMs) of 1-mercapto-8-bromooctane adsorbed on Au(lll)from aqueous solution. The analysis of the relative band intensity of Penning spectrum indicates that the molecule stand up right to the substrate surface at room temperature. Upon heating, the molecule becomes tilted in the layer.

VI-L-3 Thickness-Dependent Orientation of the Pendant Phenyl Group at the Surface of Polystyrene Thin Films

UENO, Nobuo; AZUMA, Yasushi; TSUTSUI, Masahiko[1]; OKUDAIRA, Koji K.[1]; HARADA, Yoshiya[1]
*(*Chiba Univ.)*

This paper reports on experimental evidence showing that the take-off angle dependence of the photoelectron intensity from the top n band of a polystyrene thin film, onginating from the pendant phenyl group, depends on the film thickness. The result indicates that the orientation of the phenyl group at the film surface changes with the film thickness. Theoretical analysis of the observed angular distribution using the single scattennng approximation combined with molecular orbital calculation (SS/MO) showed that the phenyl groups at the film surface become perpendicular oriented for a thicker film. The present finding suggests the possibility that thc surface property of a thin film of a pendant group polymer can be controlled by changing the film thickness.

VI-L-4 Structure of Copper- and H_2-phthalocyanine Thin Films on MoS_2 Studied by Angle Resolved Ultraviolet Photoelectron Spectroscopy and Low Energy Electron Diffraction

OKUDAIRA, Koji K.[1], HASEGAWA, Shinji; ISHII, Hisao[2]; SEKI, Kazuhiko[2]; HARADA, Yoshiya; UENO, Nobuo
([1]Chiba Univ., [2]Nagoya Univ.)

Angle-resolved ultraviolet photoelectron spectra (ARUPS) of copper phthalocyanine (CuPc) and metal-free phthalocyanine (H_2Pc) films (thickness from monolayer to 50-80 Å) on cleaved MoS_2 substrates were measured using monochromatic synchrotron radiation. Observed take-off angle (θ) and azimuthal angle (ϕ) dependencies of the top π band intensity were analyzed quantitatively by the single-scattering approximation theory combined with molecular orbital calculations. The analysis indicated that the molecules lie ffat on the MoS_2 surface in monolayer films of CuPc and H_2Pc. The azimuthal orientation of the molecules (angle between molecular axis and surface crystal axis of MoS_2), was found to be about –7°, –37°, or –67° for both monolayer films of CuPc and H_2Pc. In the azimuthal orientation, the analyses indicated that there are only molecules with conterclockwise rotation, although both clockwise and counterclockwise rotations are expected. From the low energy electron diffraction, the two-dimensional lattice stsucture of the monolayer film was obtained. On the basis of these two kinds of experimental results, the full structure of the monolayer film, the two dimensional lattice and the molecular orientation at the lattice points, was determined. Furthermore, for the thick films it is found from the analyses of ARUPS that CuPc and H_2Pc molecules tilt about 10° from the surface plane.

VI-L-5 Electronic Structure of Poly(1,10-phenanthroline-3,8-diyl) and Its K-doped State Studied by Photoelectron Spectroscopy

MIYAMAE, Takayuki; UENO, Nobuo; HASEGAWA, Shinji; SAITO, Yutaka[1]; YAMAMOTO, Takakazu[1]; SEKI, Kazuhiko[2]
([1]Tokyo Inst. Tech., [2]Nagoya Univ.)

Ultaviolet photoelectron spectra were measured using synchrotron radiation for thin films of poly(1,10-phenanthroline-3,8-diyl) (PPhen) and its potassium-doped state. Upon potassium doping of PPhen, two new states, which could be assigned to bipolaron bands, appear in the originally empty energy gap. The electronic structure of the neural and potassium-doped states was theoretically analyzed using single-scattering approximation combined with semiempirical molecular orbital calculations.

VI-L-6 A Differential Thermal Analysis and Ultraviolet Photoemission Study on Surface Freezing of n-Alkanes

YAMAMOTO, Yasushi[1]; OHARA, Hideaki[1]; KAJIWARA, Kotaro[1]; ISHII, Hisao[1]; UENO, Nobuo; SEKI, Kazuhiko[1]; OUCHI, Yukio[1]
([1]Nagoya Univ.)

The surface-freezing effect of pentacontane (*n*-$C_{50}H_{102}$) and tetratetracontane (*n*-$C_{44}H_{90}$) films evaporated on a copper substrate has been investigated by differential thermal analysis (DTA) simultaneously with measurements of surface-specific ultraviolet (UV) photoemission. Two anomalies in the DTA curve were observed near the bulk melting temperature, one of which has been attributed to bulk melting. Since the temperature dependence of the surface-specific UV photoemission measurement showed a corresponding stepwise increase and decrease in the photoemission current at the two anomalies observed in the DTA, we have concluded that the other phase transition peak originates from surface freezing.

VI-L-7 Angle-Resolved UPS Studies of Organic Thin Films

UENO, Nobuo

This paper describes recent progress of angle-resolved photoelectron spectroscopy using synchrotron radiation (SR-ARUPS) on organic thin films. SR-ARUPS has been growing to a new surface analysis technique which can offer concrete information on the molecular orientation at the film surface as well as on the origin of the electronic structure, both of which are important in understanding functions of organic thin films. Some examples of the experimental determination of the molecular orientation by SR-ARUPS are shown for epitaxial ultrathin films of phthalocyanines and bis(l,2,5-thiadiazolo)-*p*-quinobis (1,3-dithiole) (BTQBT). The orientation of pendant naphthalene groups at the surface of thin film of poly(2-vinyl-naphthalene) is also shown, where the comparison between the results obtained by SR-ARUPS and near edge X-ray absorption fine structure (EXAFS) spectroscopy is made in order to understand an advantage of SR-ARUPS. Furthermore, it is pointed out by showing the result on C_{60} thin film that the multicentered photoemission dominates the photoelectron intensity of thin films of large organic molecules.

VI-M Thin Film Preparation of SiO_2 by Photo-Chemical Vapor Deposition Using Vacuum Ultraviolet Radiation

Silicon dioxide has been extensively used and studied in semiconductor manufacturing applications. For such a material, conventional pyrolytic deposition occurs above 600 °C while traditional oxidation occurs at temperatures around and above 900 °C. Low temperature processing has become much more important mainly in the semiconductor industry, according to the continued reduction in device geometry. Photo-stimulated processing is very promising since the processed surfaces and growing films are not subjected to damaging ionic bombardment unavoidable in plasma-assisted processing systems. The aims of this project are to exploit the fundamental processes and to demonstrate the possibility and inherent advantages of depositing silicon dioxide at room temperature from tetraethoxyorthosilicate (TEOS: $Si\text{-}(OC_2H_5)_4$) with the use of vacuum ultraviolet radiation.

VI-M-1 SiO_2 Thin Film Preparation Using Dielectric Barrier Discharge-Driven Excimer Lamps

TAKEZOE, Noritaka; YOKOTANI, Atsushi[1]; KUROSAWA, Kou; SASAKI, Wataru[1]; IGARASHI, Tatsushi[2]; MATSUNO, Hiromitsu[2]
([1]Miyazaki Univ.; [2]USHIO Inc.)

[*Appl. Surf. Sci.* **138-139**, 340 (1999)]

By suing a photochemical vapor deposition method with a Xe_2 excimer lamp (172 nm, 20 mW/cm^2 output power), silica films have been prepared by means of a single precursor from tetraethoxyorthosilicate (TEOS) at room temperature. Transparent thin films of SiO_2 obtained on sapphire and quartz single crystal substrates with a deposition rate of 0.9 nm/min. They were mainly composed of amorphous SiO_2, although small amounts of residual organic materials were contained. The refractive index was 1.476 at 632.8 nm. The surface roughness decreased with the film thickness and reached 0.2 nm-rms. These findings indicate that the VUV excimer lamp CVD is a promising method for preparing smooth, dense and fine thickness-controllable films of SiO_2 at room temperature.

VI-M-2 SiO_2 Film Coatings with VUV Excimer Lamp CVD

KUROSAWA, Kou; TAKEZOE, Noritaka; YANAGIDA, Hideaki; NOMURA, Ryo[1]; YOKOTANI, Atsushi[1]
([1]Miyazaki Univ.)

[*Mater. Res. Soc. Symp. Proc.* **555**, 167 (1999)]

Silica film coatings were demonstrated using photo-chemical vapor deposition with a 172-nm Xe excimer lamp. Tetraethoxyorthosilicate (TEOS) molecules were successfully dissociated into SiO_2 + $2C_2H_5$-OH + (residual C and H) with the 7.2-eV photons. The films were deposited onto quartz or Al_2O_3 single crystal substrates with the deposition rate of 1 nm/min. The films were uniform and smooth enough for optical applications.

VI-M-3 Thin Film Preparation Using Vacuum Ultraviolet Rare Gas Excimer Lamps

TAKEZOE, Noritaka; YOKOTANI, Atsushi[1]; KUROSAWA, Kou
([1]Miyazaki Univ.)

[Hyomen Kagaku 20, 401 (1999)]

Rare gas excimer lamps using dielectric-barrier discharge are new type of compact and high-efficient light source for vacuum ultraviolet wavelength region. Since the lamps produce incoherent and quasi-continuous radiation, uniform processing over large sample areas is expected to be possible without thermal effects and speckling or interference fringes. The purpose of this paper is to exploit a new technique of material processing by use of the newly developed incoherent rare gas excimer lamps. We will describe some findings obtained by applying the excimer lamps to preparation of silica films. A photochemical vapor deposition using Xe_2* excimer lamp has made it possible to prepare silica films by means of a single precursor process from tetraethoxyorthosilicate (TEOS) at room temperature. Transparent SiO_2 thin films were obtained with a deposition rate of 0.9 nm/min. The refractive index was 1.476 at 632.8 nm and the surface roughness reached 0.2 nm-rms. These findings indicate that the VUV excimer lamp CVD is promising method for preparing smooth and fine thickness-controllable films of SiO_2 at room temperature. We confirmed that this technique provides a very promising photo-quantum process for the fabrication of semiconductors and opt-electronic devices, and others.

VI-M-4 Photo-Dissociation Process of Tetra-ethoxyorthosilicate (TEOS) Induced by Synchrotron Radiation

YANAGIDA, Hideaki; TAKEZOE, Noritaka; KUROSAWA, Kou; YOKOTANI, Atsushi[1]; KAWASAKI, Yasuhiro[1]; MAESONO, Yoshihiro[1]; NOMURA, Ryo[1]
([1]Miyazaki Univ.)

Tetraethoxyorthsilicate (TEOS: $Si\text{-}(OC_2H_5)_4$) is one of the promising materials for preparing insulating SiO_2 thin layer in semiconductor industry. Photo-chemical vapor deposition using vacuum ultraviolet radiation provides the thin film preparation at room temperature. However the photo-dissociation process has never been exploited yet. We have a plan to exploit the detailed process, to find the most appropriate conditions, in particular for wavelength, and to make high quality SiO_2 thin film using synchrotron radiation (at the beam lines of BL-1B and BL-7B of UVSOR).

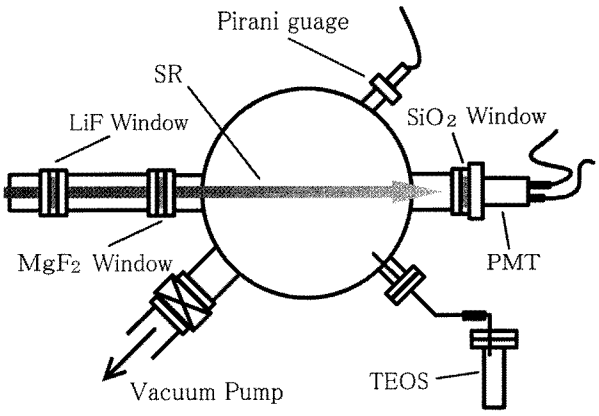

Figure 1. Schematic drawing of reaction chamber for TEOS.

VI-N Vacuum Ultraviolet Lasers and Their Applications to Surface Modification of Silica Glass

Rare gas excimers are most promising materials for coherent light sources in vacuum ultraviolet spectral region. Among them, an argon excimer laser which provides 126-nm photons has been realized only by high-energy electron beam pumping. The photon energy surmounts the band-gap energy of almost all solid-state materials and thus has a strong interaction with the materials. For an example, we have demonstrated that the 9.8-eV photons excite electrons from the valence band to the conduction band via one-photon process, resulting in desorption of oxygen atoms and crystal growth of silicon in the surfaces of silica glass and quartz crystals.

VI-N-1 The State of the Art of Rare Gas Excimer Lasers and Lamps as a Light Source for Giga-Bit Lithography

SASAKI, Wataru[1]; KUROSAWA, Kou; KUBODERA, Shoichi[1]; KAWANAKA, Jyunji[1]
([1]Miyazaki Univ.)

[*J. Photopolymer Sci. Tech.* **11**, 361 (1998)]

Coherent and incoherent light sources using rare gas excimers are reviewed from a point of view of post ArF lithography. Present status of electron beam pumped rare gas excimer lasers is reported. Potentialities of rare gas excimer lasers by discharge pumping are discussed. We have obtained laser gain of 2.2×10^{-3} cm^{-1} in Kr discharge that was very close to the threshold gain. It is pointed out that gas excimer lasers are suitable for light sources for next generation lithography after ArF lithography in the 21st century, when a compact excitation method is established. Jet discharge excimer lamps are also discussed from a point of view of an incoherent light source for lithography.

VI-N-2 Radiation Effects of Vacuum Ultraviolet Lasers on Silica Glasses

KUROSAWA, Kou; HERMAN, Peter[1]; SASAKI, Wataru[2]
([1]Univ. Toronto; [2]Miyazkai Univ.)

[*J. Photopolymer Sci. Tech.* **11**, 367 (1998)]

Excimer-laser processing can be extended to a broader and more diverse range of materials by moving to vacuum-ultraviolet (100–200 nm) laser sources such as the molecular fluorine and argon excimer lasers. The 126-nm and 157-nm output wavelengths from the argon excimer and fluorine lasers take advantages of the extremely high photon-energy, the high opacity in most materials, and short pulse duration to minimize thermal loading of target surfaces. The lasers readily drive photochemical interactions. The 126-nm photons induce oxygen desorption and silicon precipitation both in high purity silica glass and crystalline quartz. The 157-nm photons readily etch off the surfaces in vacuum ultraviolet-grade silica glass and crystalline quartz.

VI-N-3 X-Ray Emission Spectroscopic Studies of Silicon Precipitation in Surface Layer of SiO_2 Induced by Argon Excimer Laser Irradiation

KUROSAWA, Kou; HERMAN, Peter[1]; KURMAEV, E.[2]; SHAMIN, S.[2]; GALAKHOV, V.[2]; TAKIGAWA, Yasuo[3]; YOKOTANI, Atsushi[3]; KAMEYAMA, Akihiro[3]; SASAKI, Wataru[3]
([1]Univ. Toronto; [2]Inst. Met. Phys., Russia; [3]Miyazaki Univ.)

[*Appl. Surf. Sci.* **126**, 83 (1998)]

The ultra-soft X-ray emission spectra were taken from surfaces of bulk silica glass and silica glass films exposed to an argon excimer laser (λ = 126 nm) and composed with the spectra taken from the virgin surfaces. The precipitation of crystalline silicon is found to take place in thin surface layers of the irradiated bulk silica glass and 15 nm film. An estimation of concentration of crystalline silicon precipitation with the depth is given on the basis of the measurements of Si $L_{2,3}$ X-ray emission spectra obtained at different accelerating voltages of the electron beam on the X-ray

tube. Based upon the precipitation conditions for these samples, we discuss the crystalline silicon precipitation mechanisms: the electronic excitation induces the bond-breaking between Si and O atoms, although there is a critical density of photons for the bond-breaking and temperature rise enhances the crystalline silicon precipitation.

VI-N-4 Polycrystalline Silicon Precipitation on SiO_2 Using an Argon Excimer Laser

OHMUKAI, Masato[1]; TAKIGAWA, Yasuo[2]; KUROSAWA, Kou
([1]Akashi College Tech.; [2]Osaka Electro-Commun. Univ.)

[*Appl. Surf. Sci.* **137**, 78 (1999)]

We are developing an argon excimer laser that oscillates at 126 nm (9.8 eV). Since the photon energy of the laser is as high as 9.8 eV, the laser can induce bond breaking in most of materials without any reactive gas or solution. We performed irradiation of an argon excimer laser on crystal and glass SiO_2, and then investigated the surfaces by means of X-ray photo-electron spectroscopy, Raman scattering, X-ray diffraction and reflection of high-energy electron diffraction measurements. The results indicate that polycrystalline silicon precipitates on the surface with a preferential orientation.

VI-O Photo-Stimulated Luminescence as Data Storage in UV to Vacuum UV Regions

Photo-stimulated luminescence is a promising process for data storage in X-ray radiation with the advantages of linear response and wide dynamic range. The fundamental mechanisms under the data storage in imaging plates using BaFBr:Eu as the photo-stimulated luminescence material have been explained to trapping electrons released from Eu impurity atoms at least for X-ray radiation. Viewing the energy diagram, we can expect the photo-stimulated process occurring even for Vacuum UV and UV radiation. We have exploited the fundamental mechanism for data storage in the imaging plate particularly for VUV and UV radiation.

VI-O-1 Response Characteristics of Imaging Plate in UV Region

YAMASHITA, Hiroshi[1]; KATTO, Masahoto[1]; OHNISI, Shunshiro[1]; KURIOKA, Yutaka[1]; TAKIGAWA, Yasuo[2]; KUROSAWA, Kou; YAMANAKA, Tatsuhiko[3]; MIYAHARA, Jyunji[4]
([1]Kinki Univ.; [2]Osaka Electro-Commun. Univ.; [3]Osaka Univ.; [4]Fuji Photo Film Co. Ltd.)

[*Rev. Laser Eng.* **26**, 812 (1998)]

An imaging plate (IP) has been developed as an image-storing medium for use in medical X-ray diagnosis. We confirmed the IP to be a good medium not only for X-ray radiation but also vacuum ultraviolet (VUV) and ultraviolet (UV) radiation. We found that the photo-stimulated luminescence (PSL) intensity showed a linear response to UV photon numbers in the range of $10^{4.5}$, and that showed saturation as the irradiated photon number increased. The sensitivity curve of the IP showed a peak at the wavelength of 200 nm and decreased at longer wavelengths. When the wavelength of the irradiated UV radiation was longer than 320 nm, the PSL intensity was too low to detect with our system. This means that the cut-off wavelength of the sensitivity was measured as 310 nm.

VI-P Nano-Structure Fabrication Using Synchrotron Radiation Stimulated Processing

Nano structures must open new windows not only for surface physics and chemistry but also for electronic and photonic devices. Synchrotron radiation stimulated surface chemical reactions have been a most promising way to fabricate nano structures, because they offer a process with the advantages of high-site selectivity by core electron excitation and also free-of damage with atomic scale. Since a new beam line with higher flux is required for the processings, we have been designing and constructing BL-4A2 beam line for the nano structure fabirication.

VI-P-1 Design and Construction of BL-4A2 Beam Line for Nano-Structure Processing

TAKEZOE, Noritaka; YANAGIDA, Hideaki[1]; KUROSAWA, Kou; URISU, Tsuneo; MEKARU, Harutaka; NODA, Hideyuki; MATSUI, Shinji[2]; KANDA, Kazuhiro[2]; UCHIDA, Hiroyuki[3]
([1]Miyazaki Univ.; [2]Himeji Inst. Tech.; [3]Toyohashi Univ. Tech.)

We have been constructing a new beam line BL-4A2 which consists of white ray beam, ultra-high vacuum scanning tunneling microscope (UHV-STM) and photo-stimulated reaction chamber. In near future, we are going to join a near field optical microscope for monitoring optical properties with the atomic scale to

them. Figure 1 shows the outline of the beam line, which consists of pre-focusing mirror (M1), secondary mirror (M2), monitor port, two differential pumping ports, reaction chamber and STM. An elliptically bent cylindrical mirror made of a quartz coated with platinum is used as the pre-mirror. The reflected beam is focused at a point of 12.7 m down stream from the center of the pre-mirror and has a sopt size of 8×6 mm^2. Low energy electron diffraction (LEED) is installed in the reaction chamber for in-situ characterization of substrate surfaces and also STM is for observation of the surface processes with atomic scale. We have a plan to make a photonic band-gap structures in a SiO_2 planer waveguide and study evanescent light from the waveguide surfaces with near field optical microscope.

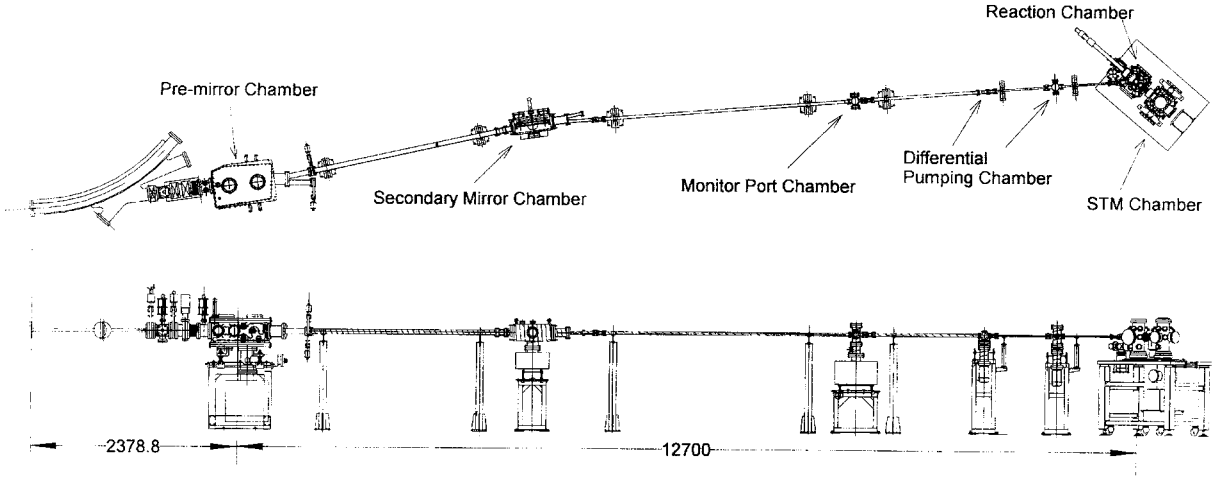

Figure 1. Schematic drawings of the BL-4A2 beam line with a reaction chamber and STM.

VI-Q Desorption Induced by Electronic Transitions from Cryogenic Surfaces

Desorption process of particles from cryogenic surfaces are studied using synchrotron radiation in vacuum ultraviolet region. As a result of decay processes after an electronic excitation of surface layers by synchrotron radiation, various kinds of particles are released from the surface. Cryogenic substrates such as solid rare gases have particular excitation channels for the desorption of electronically excited neutral particles that are pronounced at the creation energy region of exciton. Experiments are performed at BL2B1 and BL5B of UVSOR. We discuss the mechanisms of excitation, energy and angular distribution of desorbed species, incident energy dependence of desorption yield, correlation between particle emission and photon emission, and so on.

VI-Q-1 Desorption of Excimers from the Surface of Solid Ne by Low Energy Electron or Photon Impact

HIRAYAMA, Takato[1]; HAYAMA, Akira[1]; ADACHI, Takashi[1]; ARAKAWA, Ichiro[1,2]
([1]Gakushuin Univ.; [2]IMS)

Desorption of excited dimers Ne_2* in $^3\Sigma_u$ state from the surface of solid Ne initiated by the creation of a valence exciton was confirmed experimentally using low energy electron and monochromatic VUV light as excitation sources. The kinetic energy of desorbed excimer (Ne_2* $^3\Sigma_u$) was (0.2 ± 0.1) eV, which is consistent with a recent quantum mechanical calculation. It is found that the vibrational relaxation of a molecular type exciton is a slow process compared to the time scale of desorption. Desorption of excimers at the excitation of the first order surface exciton was found to be inefficient compared to that by the creation of bulk excitons, which is in striking contrast to the case of the excited atom desorption. The mechanism of excimer desorption can be explained by a cavity ejection model as in the atomic desorption case.

VI-Q-2 Photon Stimulated Ion Desorption from Solid Rare Gases in the Core Excitation Region

SAKURAI, Makoto; MASE, Kazuhiko; NAGASONO, Mitsuru; TANAKA, Shin-ichiro

Ion desorption from solid rare gases was measured by the irradiation of synchrotron radiation in the core excitation region. Experiments were performed in a UHV chamber at BL-2B1. Solid rare gases were prepared on gold-plated copper substrate, which was attached at the end of a flow type liquid He cryostat. Partial electron yield (PEY) and total ion yield (TIY) spectra of condensed Ar and Xe were measured using an Auger electron-photoion coincidence spectrometer.

Typical PEY and TIY spectra of condensed Ar measured around the energy range of Ar 2p excitation exhibit very similar waveforms, and ion yield is relatively high compared to the intensity of emitted electrons. The measured electron corresponds to LMM Auger electron (~210 eV). The time of flight spectrum of desorbed ions in the coincidence with Auger electrons showed no observable peaks. We obtained similar results for condensed Xe at 3d excitation (~680 eV). These features suggest that ion desorption from solid rare gases in the core excitation region is dominated by the interaction between the secondary electrons and desorbing ions.

VI-R Structure and Vibrational Spectra of Molecules Physisorbed on Metal Surfaces

Molecular layers physisorbed on metal surfaces at low temperature show specific structures which depend on the interaction between molecules and substrate, and vibrational spectra for physisorbed molecules reveal the details of the interaction. We use dynamical analysis of low-energy electron diffraction (LEED) to investigate the structure of adsorbed layers, and high-resolution electron energy loss spectroscopy has been utilized for vibrational spectroscopy for adsorbed molecules. As a complemental method for vibrational spectroscopy of surfaces, infrared reflection absorption spectroscopy will be combined with our experimental system. A new cryogenic sample holder for surface vibrational spectroscopy is also under development in order to provide a substrate at less than 4.2K.

VI-R-1 Upgraded Infrared Beamline BL6A1 at UVSOR

SAKURAI, Makoto; OKAMURA, Hidekazu[1]; WATANABE, Katsumi[1]; NANBA, Takao[1]; KIMURA, Shin-ichi[1]; KAMADA, Masao
([1]Kobe Univ.)

[*J. Synchrotron Radiat.* **5**, 578 (1998)]

BL6A1, a far-infrared (FIR) beamline at UVSOR originally built in 1986, has been upgraded recently. The upgrade included the introduction of a second FT-IR spectrometer, and now it is possible to cover the entire FIR-IR range (3 cm^{-1} to 10000 cm^{-1}) in one sequence of measurements, without having to open the sample chamber; the beamline has become a more convenient and powerful experimental station than before. The upgrade is also expected to enable such experiments as IR studies of molecules adsorbed on the

solid surfaces, and time-resolved IR spectroscopies.

VI-R-2 Development of High Sensitivity EELS

SAKURAI, Makoto

Electron energy loss spectroscopy (EELS) is a powerful tool for the structural analysis of molecules adsorbed on a solid surface. However, since ordinary EELS system uses a single channel electron analyzer, the measurement time for one spectrum usually amount to several minutes. This has been a disadvantage of EELS for real time analysis of surface reaction. We developed a new electron analyzer for EELS. The analyzer is a simulated hemispherical analyzer with a position sensitive detector. The components are made of aluminum, and mean radius of the deflector is 104 mm. The detector has CR chain type anode, and the signal is stored to a histogramming memory via position analyzer. The spectrum can be measured as frequent as every 10ms. This feature makes it possible to perform a time-resolved measurement of repetitive reaction processes. The analyzer and an cylindrical double pass monochromator are mounted on a rotatable stage, and they are installed in a vacuum chamber (600ϕ). Control program written in Visual Basic for the data acquisition system has been developed.

VI-S Structure and Vibrational Spectra of Molecules on Metal Surfaces

Adsorption structure of the adsorbed molecules is one of the most fundamental information to understand the reaction of the molecules on the surface, which is useful for calculating the electronic structure of the system and understanding the elementary processes such as desorption, dissociation or diffusion. Understanding the elementary processes further enables us to understand more complex reactions such as catalysis. Nitric oxide (NO) on the Pt(111) surface is a prototype of catalytic process of the exhaust gas of automobiles. In spite of many efforts, its adsorption structure has not been determined yet. Dynamical analysis of low-energy electron diffraction (LEED) and direct observation by scanning tunneling microscopy (STM) are utilized to investigate the structures of adsorbed molecules in various conditions. Vibrational spectra, which is closely related to adsorption structure, are also utilized to determine the structures correctly.

VI-S-1 Adsorption Structures of NO on Pt(111) Investigated by Scanning Tunneling Microscopy

MATSUMOTO, Masuaki; TATSUMI, Natsuo[1]; FUKUTANI, Katsuyuki[1]; OKANO, Tatsuo[1]; YAMADA, Toshiyuki[2]; MIYAKE, Koji[2]; HATA, Kenji[2]; SHIGEKAWA, Hidemi[2]
([1]IIS, Univ. Tokyo; [2]Tsukuba Univ. and CREST)

[*J. Vac. Sci. Technol., A* **17**, 1577 (1999).]

The adsorption structure of nitric oxide (NO) on Pt(111) was studied at 10 and 70 K by scanning tunneling microscopy (STM). The island growth modes at both temperatures are similar except for the domain size of the 2×2 structure. In these low temperature region, two phases can coexist at medium coverages. These phases are assigned to the two NO species occurring at different stretching-vibrational frequencies observed in the previous vibrational spectroscopic studies. The relative location of two different species observed by STM and its stretching-vibrational frequencies suggests that the adsorption sites of NO on the Pt(111) surface at low and high coverages correspond to the hollow and the on-top sites, respectively.

VI-S-2 Dynamical LEED Analyses of the Pt(111)-p(2×2)-NO Structures

TATSUMI, Natsuo[1]; MATSUMOTO, Masuaki; AIZAWA, Hideaki[2]; TSUNEYUKI, Shinji[3]; FUKUTANI, Katsuyuki[1]; OKANO, Tatsuo[1]
([1]IIS, Univ. Tokyo; [2]Univ. Tokyo; [3]ISSP, Univ. Tokyo)

[*J. Vac. Soc. Jpn.* **42**, 572 (1999).]

Adsorption structures of NO molecules on a Pt(111) surface at low temperatures have been studied using low-energy electron diffraction (LEED). At 150 K a 2×2 LEED pattern appears at exposures higher than 0.2 L. With increasing exposure, the LEED spots get sharper, indicating two-dimensional island growth of adsorbed NO. The LEED I-V spectra measured at 0.4 L are different from those at 3 L, suggesting the presence of two kinds of 2×2 structure. The LEED I-V analysis performed for the 2×2 at 0.4 L strongly supports that NO is adsorbed at a threefold fcc hollow site. For the I-V curves of 2×2 at 3 L, the fcc hollow site model calculation does not fit the experimental I-V curve, suggesting that a different 2×2 structure grows after the first 2×2 structure is completed.

VI-T Ultraviolet, Visible and Infrared Spectroscopy of Solids

Work of ultraviolet (UV), visible (VIS) and infrared (IR) spectroscopy of solids have been proceeded. These are mainly performed using synchrotron radiation (beamlines BL7B and BL1B at UVSOR), owing to the wide wavelength continuity of synchrotron radiation with no structure.

VI-T-1 Reconstruction of BL7B for UV, VIS and IR Spectroscopy with a 3 m Normal-Incidence Monochromator

FUKUI, Kazutoshi; NAKAGAWA, Hideyuki[1]; SHIMOYAMA, Iwao[2]; NAKAGAWA, Kazumichi[2]; OKAMURA, Hidekazu[2]; NANBA, Takao[2]; HASUMOTO, Masami; KINOSHITA, Toyohiko[3]
([1]Fukui Univ.; [2]Kobe Univ.; [3]Univ. Tokyo)

[*J. Synchrotron Radiat.* **5**, 836 (1998)]

The beamline BL7B at the UVSOR facility for solid-state spectroscopy is currently under reconstruction. This reconstruction mainly involves the replacement of the 1 m Seya-Namioka-type monochromator (50-600 nm) with a 3 m NIM (modified version of McPherson model 2253), which covers the 50-1000 nm range with three gratings. The deviation angle of the gratings is 15°. For linear and circular polarization experiments, the beamline optics consist of a two-grazing-incidence (87.5°) pre-mirror system and a normal-incidence (15°) post-mirror.

VI-T-2 Absorption and Luminescence Spectra of Amorphous CdI_2 Thin Films

FUKUI, Kazutoshi; ASAKURA, Kenji[1]; NIIMI, Ken-ichi[1]; ISHIZUE, Ikuto[1]; NAKAGAWA, Hideyuki[1]
([1]Fukui Univ.)

[*J. Electron Spectrosc. Relat. Phenom.* **101-103**, 299 (1999)]

Absorption and luminescence spectra of amorphous CdI_2 thin film were measured at liquid nitrogen temperature. Two emission bands were observed at 2.3 and 3.1 eV, and the intensity ratio between them depends on the excitation energy. The 3.1 eV emission is explained in terms of the MX_6 model which explains the emission mechanism of the CdI_2 crystal, but the other is not explained.

VI-T-3 Optical Study of the Metal-Nonmetal Transition in $Ni_{1-\delta}S$

OKAMURA, Hidekazu[1]; NAITOH, Jun[1]; NANBA, Takao[1]; MATOBA, Masanori[2]; NISHIOKA, Masaya[2]; ANZAI, Shunichiro[2]; SHIMOYAMA, Iwao[1]; FUKUI, Kazutoshi; MIURA, Hiroshi[3]; NAKAGAWA, Hideyuki[3]; NAKAGAWA, Kazumichi[1]; KINOSHITA, Toyohiko[4]
([1]Kobe Univ.; [2]Keio Univ.; [3]Fukui Univ.; [4]Univ. Tokyo)

[*Solid State Commun.* **112**, 91 (1999)]

Optical reflectivity spectra of the hexagonal $Ni_{1-\delta}S$ have been measured to study its electronic structures, in particular those associated with the metal-nonmetal transition in this compound. Samples with $\delta \sim 0.002$ and 0.02 are studied, which have transition temperature $T_t \sim$ 260 K and 150 K, respectively. Upon the transition, a pronounced dip appears in the infrared region of the reflectivity spectra. The optical conductivity spectra suggest that the nonmetallic phase is a carrier-doped semiconductor with an energy gap of ~ 0.2–0.3 eV. The spectra also show that the gap becomes larger with decreasing temperature, and smaller with increasing δ. It is found that the overall spectrum in the nonmetallic phase can be explained in terms of a charge-transfer semiconductor, consistent with recent theoretical and photoemission studies of NiS.

VI-U Electronic Structure and Optical Properties of III-V Nitrides

The III-V nitrides (GaN, AlN and InN) and their alloys (AlGaN, InGaN and AlInN) are promising for optoelectronic device application. They are also the attractive material series which have scientific interest because the band structure, the luminescence mechanisms, excitons, *etc.* are still not well known. We mainly investigate their band structures using vacuum ultraviolet and soft X-ray monochromators combined with synchrotron radiation light source (UVSOR). Since the core levels are strictly localized in space, core absorption spectrum gives us the site-specific information which is a useful method to investigate the binary or ternary compounds.

VI-U-1 Soft X-ray Absorption Study of III-V Nitrides

FUKUI, Kazutoshi; HIRAI, Ryousuke[1]; YAMAMOTO, Akio[1]; NAOE, Syun-ichi[2]; TANAKA, Satoru[3]
([1]Fukui Univ.; [2]Kanazawa Univ.; [3]Hokkaido Univ.)

[*Jpn. J. Appl. Phys., Part 1* **38**, 538 (1999)]

The soft X-ray absorption measurements around nitrogen K and aluminum K edge of the wurtzite AlN, GaN and their ternary compounds AlGaN have been performed. The incidence light angle dependence of the absorption spectra were clearly observed in all samples. A numerical component analysis is presented to separate the experimental K-absorption spectra into three partial spectra which correspond to in-plane, out-

of-plane and angular independent components of the unoccupied *p* partial density of states.

Reference

1) W. R. L. Lambrecht, S. N. Rashkeev, B. Segall, K. Lawniczak-Jablanska, T. Suski, E. M. Gullikson, J. H. Underwood, R. C. C. Perera, J. C. Rife, I. Grzegory, S. Porowski and D. K. Wickenden, *Phys. Rev. B* **55**, 2612 (1997).

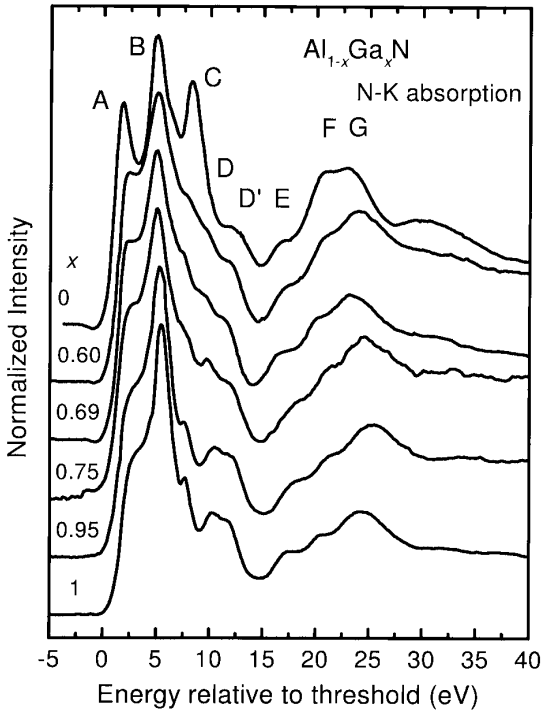

Figure 1. Normal incidence nitrogen K absorption spectra of $Al_{1-x}Ga_xN$. The energy scale is relative to the threshold energy. The labels *A* to *G* correspond to those for GaN in Reference 1. The intensity of each spectrum is normalized at the peak *B*.

VI-V Site-Specific Fragmentation Following Core-Level Photoexcitation

Monochromatized synchrotron radiation can excite core electrons of an atom in a specific chemical environment selectively, discriminating the core electrons from those of like atoms having different chemical environments. This site-specific excitation often results in site-specific fragmentation, which is of importance in understanding localization phenomena in chemical reactions and which is potentially useful for synthesizing materials through selective bond breaking. Synchrotron radiation can indeed play the part of an optical knife for molecules. When bond dissociation around an atomic site is required in the synthesis, one can use the optical knife that has the photon energy corresponding to the specific excitation of that site. To elucidate the site-specific fragmentation, we have used photoemission spectroscopy and the energy-selected-photoemission photoion coincidence method to study site-specific phenomena in the C:1s and Si:2p photoexcitation of organic and organosilicon molecules condensed on a Si surface and in the vapor phase.

VI-V-1 Site-Specific Phenomena in Si:2p Core-Level Photoionization of $X_3Si(CH_2)_nSi(CH_3)_3$ (X = F or Cl, *n* = 0–2) Condensed on a Si(111) Surface

NAGAOKA, Shin-ichi; MASE, Kazuhiko[1]; NAGASONO, Mitsuru[2]; TANAKA, Shin-ichiro[3]; URISU, Tsuneo; OHSHITA, Joji[4]; NAGASHIMA, Umpei[5]
([1]KEK-PF; [2]MAX-lab; [3]Nagoya Univ.; [4]Hiroshima Univ.; [5]Natl. Inst. Adv. Interdisciplinary)

[*Chem. Phys.* in press]

We used photoelectron spectroscopy and the energy-selected-photoelectron photoion coincidence (ESPEPICO) method to study site-specific phenomena in the Si:2p photoionization of $X_3Si(CH_2)_nSi(CH_3)_3$ (X = F or Cl, *n* = 0–2) condensed on a Si(111) surface. The site-specific excitation and the occurrence of different chemical shifts at two Si sites were revealed in the total electron-yield spectra and the photoelectron spectra of $F_3Si(CH_2)_nSi(CH_3)_3$ (*n* = 1,2), although they were not clearly revealed in those of $Cl_3SiSi(CH_3)_3$. We conclude that these site-specific phenomena are easily observed in molecules in which the two Si sites are located far apart and in which electron migration between the two Si-containing groups does not occur. This was supported by our ab initio calculation. Site-specific fragmentation was revealed in the ESPEPICO spectrum of $F_3SiCH_2CH_2Si(CH_3)_3$, although it was negligible for $Cl_3SiSi(CH_3)_3$ and was less remarkable in $F_3SiCH_2Si(CH_3)_3$ than in $F_3SiCH_2CH_2Si(CH_3)_3$. Site-specific fragmentation also occurred when the two Si sites were located far apart.

VI-V-2 Ion Desortpion Induced by Core-Electron Transitions Studied with Electron-Ion Coincidence Spectroscopy

MASE, Kazuhiko[1]; TANAKA, Shin-ichiro[2]; NAGAOKA, Shin-ichi; URISU, Tsuneo
([1]KEK-PF; [2]Nagoya Univ.)

In a study of $CF_3CH(OH)CH_3$ chemisorbed on a Si(100) surface using photoelectron photoion coincidence (PEPICO) spectroscopy, site-specific ion desorption is directly verified, that is, F^+ desorption is predominant for C:1s photoionization at the CF_3- site, while H^+ desorption is predominantly induced by C:1s photoionization at the -CH_3 site. This study demonstrates that PEPICO spectroscopy combined with synchrotron radiation is a novel and powerful tool for the study of ion desorption induced by core-electron excitations and that it is also a prospective method to investigate the electronic structure of the specific sites responsible for ion desorption.

VI-V-3 Development of Electron-Ion Coincidence Spectroscopy for Study of Surface and Vapor-Phase Dynamics

MASE, Kazuhiko[1]; NAGAOKA, Shin-ichi
([1]KEK-PF)

An electron-ion coincidence spectrometer for vapor-phase dynamics study is being built now. The equipment consists of an electron gun, a cylindrical mirror analyzer (CMA) and a time-of-flight ion mass analyzer (TOF-MS). Sample gas is excited with the electron beam and the CMA analyzes energy of emitted or scattered electrons. TOF spectra of desorbed ions are measured with a multichannel scalar taking the energy-analyzed electron signal as the starting trigger.

VI-W Study on RF-Photocathode for Compact X-Ray Sources

Electron storage rings are useful and practical devices as x-ray sources because which produce a number of photons owing to high electron current and various insertion devices. However, these synchrotron radiation facilities usually occupy large area and cost much. So that there have been many works to investigate more compact x-ray sources such as x-ray lasers and free electron lasers. It is also useful to use laser undulator radiation or backward Compton scattering caused by the interactions of electron beams with laser photons, if we provide enough electrons to produce practical intensity of x-rays. RF-photocathode would produce dense electron beam so that it is a useful candidate of a electron source. It is necessary to search good materials as the photocathode for construction of a practical compact x-ray source. Cesium telluride has reported to have a good quantum efficiency, we study about it.

VI-W-1 Measurement of Quantum Efficiency of Cesium Telluride as a Photocathode

TAKASHIMA, Yoshifumi; KOBAYAKAWA, Hisashi[1]; KIMURA, Kenichi[1]; SUGIYAMA, Harue[1]; FURUTA, Fumio[1]; NAKANISHI, Tsutomu[1]; OKUMI, Shoji[1]; TOGAWA, Kazuaki[1]; SUZUKI, Chihiro[1]; NAKAMURA, Shinsuke[1]; WADA, Kouji[1]; YAMAMOTO, Masahiro[1]; NISHITANI, Tomohiro[1]; YOSHIOKA, Masakazu[2]; MATSUMOTO, Hiroshi[2]
([1]Nagoya Univ.; [2]KEK)

The photocathode for a x-ray source is required to have high quantum efficiency for production of practical intensity of x-rays. There have been a number of works[1-4] to test materials as photocathode. We used cesium telluride as the photocathode and studied quantum efficiency. Figure 1 shows a picture of the vacuum chamber in which the cathode was installed. Ultraviolet(UV) radiations, generated with a xenon lamp, were guided into diffraction grating. Monochromatic UV radiations from the grating passed through a entrance sapphire window of the vacuum chamber, then focused on the photocathode. Cesium telluride was made on a surface of a molybdenum block by vacuum evaporation method. Negative constant voltage of 100V was supplied to the photocathode.

Electric current flowing into the cathode was measured to derive the quantum efficiency which is shown in Figure 2 with wavelength of injected UV radiations. The maximum quantum efficiency is about 10% and is kept longer than hundred hours. For the further study, we should supply RF voltage and test the cathode whether it has a good performance as this experiment.

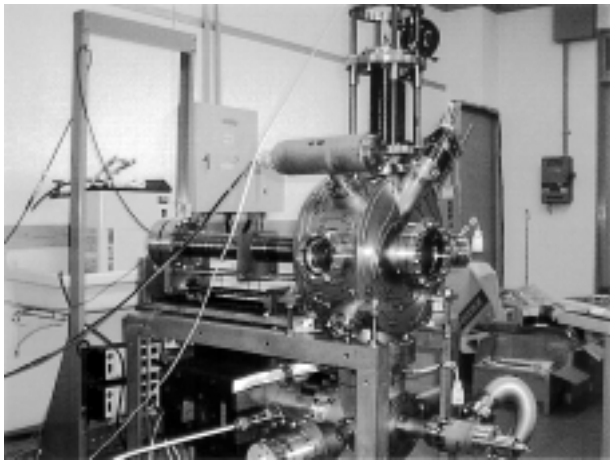

Figure 1. Vacuum chamber in which there is a photocathode. UV radiation is injected on the photocathode through one of a viewing port.

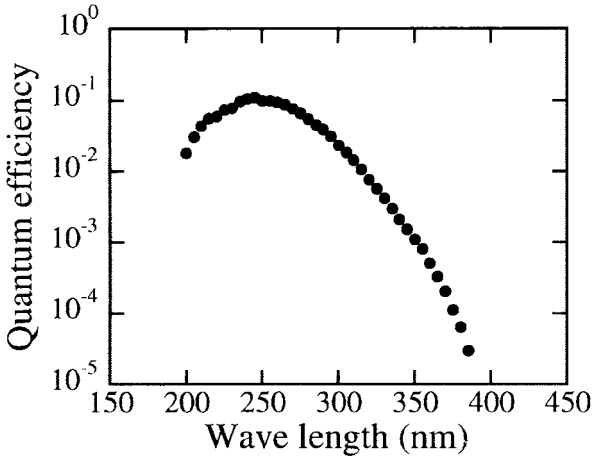

Figure 2. Quantum efficiency of cesium telluride with wavelength of injected UV radiations.

Reference

1) S. W. Downey, L. A. Buita, D. C. Moir, T. J. Ringler and J. D. Saunders, *Appl. Phys. Lett.* **49**, 911 (1986).
2) A. Septier, F. Sabary and J. C. Dudek, *Nucl. Instrum. Methods Phys. Res., Sect. A* **304**, 392 (1991).
3) Y. Yamaoka *et al.*, *Proceedings of the 14th Linear Accelerator Meeting* (1989).
4) R. A. Powell, W. E. Spicer, G. B. Fisher and P. Gregory, *Phys. Rev. B* **8,** 3987 (1973).